

1    **Descriptions of four new species of**  
2    ***Minyomerus* Horn, 1876 sec. Jansen &**  
3    **Franz, 2018 (Coleoptera: Curculionidae),**  
4    **with notes on their distribution and**  
5    **phylogeny**

6    **M. Andrew Jansen<sup>1</sup> and Nico M. Franz<sup>2</sup>**

7    <sup>1</sup>**School of Life Sciences, 427 E Tyler Mall, PO Box 874501, Tempe, AZ 85287**

8    <sup>2</sup>**ASU Natural History Collections, 734 W Alameda Dr, Tempe, AZ 85282**

9    Corresponding author:

10    M. Andrew Jansen<sup>1</sup>

11    Email address: majanse1@asu.edu

12    **ABSTRACT**

13    This contribution adopts the taxonomic concept approach, including the use of *taxonomic concept labels*  
14    (name sec. [*according to*] source) and Region Connection Calculus (RCC–5) articulations and alignments.  
15    Prior to this study, the broad-nosed weevil genus *Minyomerus* Horn, 1876 sec. Jansen & Franz, 2015  
16    (Curculionidae [non-focal]: Entiminae [non-focal]: Tanymecini [non-focal]) contained 17 species distributed  
17    throughout the desert and plains regions of North America. In this review of *Minyomerus* sec. Jansen &  
18    Franz, 2018, we describe the following four species as new to science: *Minyomerus ampullaceus* sec.  
19    Jansen & Franz, 2018 (henceforth: [JF2018]), **new species**, *Minyomerus franko* [JF2018], **new species**,  
20    *Minyomerus sculptilis* [JF2018], **new species**, and *Minyomerus tylotos* [JF2018], **new species**. The four  
21    new species are added to, and integrated with, the preceding revision, and an updated key and phylogeny  
22    of *Minyomerus* [JF2018] are presented. A cladistic analysis using 52 morphological characters of 26  
23    terminal taxa (5/21 outgroup/ingroup) yielded a single most-parsimonious cladogram (Length = 99 steps,  
24    Consistency Index = 60, Retention Index = 80). The analysis reaffirms the monophyly of *Minyomerus*  
25    [JF2018] with eight unreversed synapomorphies. The species-group placements, possible biogeographic  
26    origins, and natural history of the new species are discussed in detail.

27    **INTRODUCTION**

28    This phylogenetic study follows Jansen & Franz (2015) in the use of the taxonomic concept approach; see  
29    Franz & Peet (2009), Franz et al. (2016a,b). Accordingly:

- 30    1. *Taxonomic concept labels* – i.e., the taxonomic name sec. (*according to*) author or source (year) –  
31    are used whenever we identify one specific usage of the taxonomic name. Examples: *Minyomerus*  
32    Horn, 1876 sec. Jansen & Franz, 2015 (henceforth: [JF2015]) and *Minyomerus* Horn, 1876  
33    sec. Jansen & Franz, 2018 (henceforth: [JF2018]). We also employ this convention to express  
34    nomenclatural relationships.
- 35    2. Solely the taxonomic name – without the sec. annotation – is used to refer to the cumulative  
36    history (origin to present) of taxonomic concept labels in which that name participates. Example:  
37    *Minyomerus* Horn, 1876.
- 38    3. The annotation [non-focal] is added to taxonomic names whose meanings are not under scrutiny in  
39    the present context; such as names for higher-level weevil groups and associated plants (exempting  
40    common names). Example: Tanymecini Lacordaire, 1863 [non-focal].

41    The weevil genus *Minyomerus* Horn, 1876 [JF2018] remains currently assigned to the tribe Tanymecini  
42    Lacordaire, 1863 [non-focal], subtribe Tanymecina Lacoirdaire, 1863 [non-focal] (Curculionidae [non-

43 focal]: Entiminae [non-focal] – higher-level classification in accordance with Alonso-Zarazaga & Lyal  
44 1999 and Bouchard et al. 2011). A recent phylogenetic revision of the genus *Minyomerus* [JF2015]  
45 recognized a total of 17 described species, distributed throughout the desert and plains regions of North  
46 America (Jansen & Franz 2015).

47 Members of the genus *Minyomerus* [JF2018] are phytophagous, and may be found on a variety of  
48 host plants, especially the creosote bush *Larrea tridentata* (DC) Coville [non-focal] (Zygophyllaceae  
49 [non-focal]), broomweed *Gutierrezia Lagasca* [non-focal] (Asteraceae [non-focal]), sagebrush *Artemisia*  
50 Linnaeus [non-focal] (Asteraceae [non-focal]), and occasionally on other various members of Asteraceae  
51 [non-focal] (Jansen & Franz 2015). While many species appear to be generalists, the adults are consis-  
52 tently observed on the leaves and branches of the host, feeding on the leaf tissue. All other life stages  
53 remain unknown. Species of *Minyomerus* [2018] are commonly found in deserts throughout western  
54 North America; including the Mojave, Sonoran, Chihuahuan, and Great Basin Deserts. However, their  
55 distributional range extends throughout the semi-arid regions of the Great Plains, the Colorado Plateau,  
56 and Baja California, México (O'Brien & Wibmer 1982, Jansen & Franz 2015). The adults are flightless,  
57 as the hind wings and associated flight structures of all species are either greatly reduced or not readily  
58 apparent in dissection.

59 *Minyomerus* [JF2018] belongs to the broad-nosed weevils, subfamily Entiminae [non-focal], on the  
60 basis of having a short, broad rostrum and dehiscent mandibular process (Marvaldi 1997, Anderson 2002,  
61 Oberprieler et al. 2007, 2014, Marvaldi et al. 2014). The adults are clothed in appressed, circular scales,  
62 generally in earth-tones from white to dark brown, with sub-recumbent to erect, interspersed setiform  
63 scales ("setae") arranged in rows on the elytral intervals. Their body length can range from 2.8 mm to 6.0  
64 mm (Jansen & Franz 2015). The genus has been classified in the tribe Tanymercini [non-focal] based on  
65 the presence of post-ocular vibrissae that project anteriorly from the anterior prothoracic margin, although  
66 the exact placement and sister taxa of this genus within the tribe are currently unknown (Howden 1959,  
67 1970, 1982, Jansen & Franz 2015).

68 *Minyomerus* [JF2015] was circumscribed by a unique combination of synapomorphic traits, described  
69 by Jansen & Franz (2015) as follows:

- 70 1. The integument is covered by appressed scales that are sub-circular and overlap posteriorly.
- 71 2. The nasal plate is present as a broad, scale-covered, chevron-shaped ridge demarcating the epistoma.
- 72 3. A sulcus posteriad of nasal plate is present.
- 73 4. The scrobe is sub-equal in length to the funicle and club combined.
- 74 5. The head is directed slightly ventrally.
- 75 6. The metatibial apex lacks setiform bristles yet displays bristles that are shorter to sub-equal in  
length to the surrounding setae and conical to lamelliform.
- 76 7. The mesotarsi are slightly shorter than the mesotibiae.
- 77 8. All tarsi lack pads of setiform setae but have stout, spiniform setae.

79 The following additional characters are useful for identifying members of *Minyomerus* [JF2018],  
80 especially when differentiating the former from other genera of Tanymercini [non-focal] that may be  
81 found together in the same desert habitats; viz. *Isodrusus* Sharp, 1911 [non-focal], *Isodacrys* Sharp, 1911  
82 [non-focal], and *Pandeleteinus* Champion, 1911 [non-focal] (see also Anderson 2002):

- 83 1. The intercoxal process of the prosternum is medially divided into two halves, with the procoxae  
84 apparently contiguous in most.
- 85 2. The elytral humeri are rounded rather than angled and protruding.
- 86 3. The profemora are not dilated and lack spines.
- 87 4. The protibiae are ventrally excavated by a longitudinal groove or concavity.
- 88 5. A distinct scrobe is present and directed ventrad of the eye, with a more or less apparent tooth  
formed by an overhang of the dorsal margin.

90 Following the publication of a monographic revision of *Minyomerus* [JF2015], we have discovered  
91 four additional, undescribed species. These are known to us only from limited numbers of specimens, yet  
92 are well circumscribed by – i.e., intensionally included in (see Franz & Peet 2009) – the recent generic  
93 delimitation of *Minyomerus* [JF2015]. In other words, the addition of these new species *has not* required  
94 altering the intensional, property-based definition of the genus-level concept as circumscribed in Jansen

& Franz (2015) (see **Phylogenetic Results**). Our RCC–5 alignments (see **RCC–5 Alignments**) reflect this genus-level concept congruence while also showing which classificatory and phylogenetic structures have changed (Figs. 1–3). The precise use of the taxonomic concept labels in accordance with either [JF2015] or [JF2018] is meant to minimize the creation of new taxonomic concept labels (to counter label “inflation”; see Franz & Peet (2009)), while reflecting explicitly *which* taxonomic concepts we consider as relevantly new and unique to the present study.

Here we describe the four newly found species of *Minyomerus* [JF2018] and provide images of the holotypes and of dissected genitalia for the purpose of identification. We additionally conduct a morphological phylogenetic analysis of the genus to clarify the placement of these new taxa within *Minyomerus* [JF2018], based on the analysis provided in our previous work. An emended identification key to the species of *Minyomerus* [JF2018] is given, along with an updated species checklist. Where possible, we make note of host-plant records, and briefly discuss the geographic distributions of the herein described species. A more extensive discussion of the habits, distribution, and delimitation of the genus *Minyomerus* [JF2015] and all of its constituent species is provided in Jansen & Franz (2015).

## MATERIALS AND METHODS

The methods used in this manuscript are generally consistent with Jansen & Franz (2015). Relevant updates are detailed below. In particular, we retain the format for the species descriptions, emphasizing only those characters that vary significantly from the generic circumscription of *Minyomerus* [JF2015].

### Acquisition of museum specimens

The set of specimens used in Jansen & Franz (2015) was supplemented with material from the following collections, using the codens of Arnett Jr. et al. (1993):

**CMNC** Canadian Museum of Nature Collection, Ottawa, Ontario, Canada

**TAMU** Texas A & M University, College Station, Texas, USA

**USNM** National Museum of Natural History, Washington, D.C., USA

Georeferencing of localities was performed with Google Earth (Google Inc. 2018), following the WGS 84 standard, and reported in decimal degrees. Taxonomic names for associated host plants, as noted following each species account, are used in accordance with Munz & Keck (1973) and SEINet (2018).

### Morphological analysis

Our systematic and descriptive approach is complementary to Jansen & Franz (2015), which in turn follows Franz (2010a,b, 2012). The terminology for exterior morphology is in general accordance with de la Torre-Bueno et al. (1989). Additional morphological terms specific to broad-nosed weevils (Entiminae [non-focal]) were used as follows: Ting (1936) and Morimoto & Kojima (2003) for mouthparts; Thompson (1992) for tibial apices and abdominal segments; and Oberprieler et al. (2014) and Howden (1995) for male and female terminalia.

Measurements were taken with a Leica M205 C stereomicroscope and associated software, Leica Application Suite (LAS), version 4.1.0. Overall body length and width were measured in dorsal view as the maximum distance between the rostral and elytral apices, and the maximum width of both elytra, respectively. Rostral length was measured in dorsal view as the distance between the epistomal apex and the anterior margin of the eyes. Rostral width was measured in dorsal view as the maximum distance between the dorsal margins of the rostrum near the point of antennal insertion. Pronotal length was measured in dorsal view as the length along the midline between the anterior and posterior margins. The width of an individual elytron was measured in dorsal view as the maximum distance between the lateral margin and the elytral suture. Other length and width measurements were also performed in dorsal orientation, using the maximum length and width of the corresponding structure (profemur, protibia, elytron, and aedeagus). Images of mouthparts and terminalia were produced with the Leica microscope equipment, while habitus photographs were created with a Visionary Digital Passport II system using a Canon EOS Mark 5D II camera.

The herein newly recognized species of *Minyomerus* [JF2018] were delimited through application of the phylogenetic species concept *sensu* Wheeler & Platnick (2000). Species descriptions are in alphabetical order, rather than phylogenetic order, for ease of use. As in Jansen & Franz (2015), the

145 species descriptions represent unique, complementary accounts of the character states observed for each  
 146 species, including their intra-specific variability, but excepting characters invariant within the genus-level  
 147 concept of *Minyomerus* [JF2015]. Likewise, descriptions of males emphasize characters that are variable  
 148 and sufficiently different from those of the females to merit recognition. The key to identifying species of  
 149 *Minyomerus* [JF2018] is arranged with emphasis being placed on the most readily observable diagnostic  
 150 characters. This manuscript is arranged with the species descriptions appearing first, followed by the key  
 151 to species, and then by the phylogenetic and RCC-5 alignment results.

## 152 **Phylogenetic analysis**

153 The morphological cladistic analysis includes 26 terminal taxa; with 21 ingroup and 5 outgroup terminals.  
 154 The ingroup terminals were represented by 17 species previously assigned to *Minyomerus* [JF2015]  
 155 and four newly recognized species. In keeping with our previous analysis, we sampled outgroups fairly  
 156 broadly while remaining focused on North American lineages that are putative close relatives of the  
 157 ingroup (Jansen & Franz 2015, Nixon & Carpenter 1993).

158 Although the tribe Tanymecini [non-focal] is cosmopolitan, the majority of New World species  
 159 diversity in the tribe may be found in the subtribe Tanymecina [non-focal] (Alonso-Zarazaga & Lyal  
 160 1999). Thus, four of the five outgroup terminals are represented by species belonging to separate genera  
 161 in the Tanymecina [non-focal]; viz. *Isodacrys buchanani* Howden, 1961 [non-focal], *Isodrusus debilis*  
 162 Sharp, 1911 [non-focal], *Pandeleteinus subcancer* Howden, 1969 [non-focal], and *Pandeleteius cinereus*  
 163 (Horn, 1876) [non-focal]. Because generic relationships in the Tanymecini [non-focal] remain unresolved,  
 164 we selected a relatively far-removed taxon to root the cladogram that would nevertheless display states  
 165 applicable to the ingroup for characters under consideration (Rieppel 2007, Franz 2014). To this end we  
 166 used the North American species *Sitona californicus* (Fahraeus, 1840) [non-focal], of the tribe Sitonini  
 167 Gistel, 1856 [non-focal].

168 The character matrix was edited and phylogenetic results viewed using the WinDada and WinClada  
 169 interfaces of WinClada, respectively (Nixon 2002). Characters are numbered in accordance with  
 170 descriptive sequence used in the species accounts. A “–” symbol indicates inapplicable (character, state),  
 171 whereas a “?” symbol indicates missing information, e.g., due to the unavailability of male specimens or  
 172 insufficient specimens on hand to permit full dissections. Characters 9, 27, 39, 45 - 47, 49, and 51 were  
 173 mapped onto the preferred phylogeny using ACCTRAN optimization (see Agnarsson & Miller 2008), and  
 174 the remaining characters had an unambiguous optimization. All multi-state characters but one were coded  
 175 as additive, as explained beneath the description for each character (see **Phylogenetic Results**), based  
 176 on their alignment with the preferred phylogeny. Each alternative coding scheme was tested both alone  
 177 and in unison with the other multi-state characters to assess their impact on the topology of the preferred  
 178 phylogeny.

179 The most parsimonious tree and character state optimizations were inferred under parsimony using  
 180 NONA (Goloboff 1999). An unconstrained heuristic search was conducted using the commands: hold  
 181 100001, mult\*1000, hold/100, with mult\*max\* selected. Bootstrap support was inferred in  
 182 WinClada using the parameters of 1000 replications, hold 1000, hold/100, mult\*10,  
 183 Don't do max\*, and Save consensus. Finally, Bremer support values (Bremer 1994) and relative  
 184 fit difference (Goloboff & Farris 2001) were calculated in NONA using the commands: hold 1001,  
 185 sub 20, bs for Bremer support values, and bs\* for relative fit difference, respectively (Goloboff et al.  
 186 2008).

The motivation for providing Bremer support values and relative fit difference comes from their  
 respective interpretations, based on how the measures are calculated, *per* Goloboff & Farris (2001). Both of these indices rely on summation of the number of favorable and contradictory characters when  
 comparing a most-parsimonious tree to a suboptimal tree. If the step length of the  $i^{\text{th}}$  character ( $I$ ) of  
 $n$  total characters on the most-parsimonious tree ( $L_{MPT}$ ) is less than its corresponding step length on  
the suboptimal tree ( $L_{SUB}$ ), the character is designated as favorable ( $f_i$ ), but if the opposite is true, the  
character is designated as contradictory ( $c_i$ ), and expressed formally:

$$I = \begin{cases} f_i & L_{MPT} < L_{SUB} \\ c_i & L_{MPT} > L_{SUB} \end{cases} \quad (1)$$

Where the number of favorable ( $F$ ) and contradictory ( $C$ ) characters are defined, respectively, as:

$$F = \sum_{n=0}^i f_i \quad (2)$$

$$C = \sum_{n=0}^i c_i \quad (3)$$

Bremer support values (bsv) and relative fit difference (rfd) are then calculated simply as:

$$\text{bsv} = F - C \quad (4)$$

$$\text{rfd} = \frac{F - C}{F} \times 100 \quad (5)$$

The Bremer support value for a node thus indicates how many more characters support a node than contradict it, while the relative fit difference indicates what proportion of the favorable characters are represented by the Bremer support value. Whereas the Bremer support value is as large as the number of characters supporting the node, in excess of the contradicting characters, the relative fit difference can only vary from 0 to 100, as a proportion of the number of supporting characters. By providing both measures, one may quickly discriminate, for example, between a node supported by 4 characters but contradicted by 1 character (bsv = 3, rfd = 75), and a node supported by 10 characters but contradicted by 7 characters (bsv = 3, rfd = 30).

### Taxonomic annotations and RCC–5

In accordance with Jansen & Franz (2015), we use the symbol “=” to indicate nomenclatural synonymy (objective/subjective); and the RCC–5 symbols {==, >, <, ><, !} indicate taxonomic concept articulations. The annotations (INT) and (OST) indicate intensional and ostensive readings of articulations, and AND is used to connect multiple simultaneously recognized provenance relationships. Two *intensional* alignments are produced as part of this review, i.e., one that captures the non-/congruence of *Minyomerus* [JF2018] versus *Minyomerus* [JF2015] represented as rank-only classifications (Fig. 1), and another that represents these as fully bifurcated phylogenies with newly assigned clade concept labels, shown in whole-concept resolution (Fig. 2) and in split-concept resolution (Fig. 3); see Franz et al. (2018).

A detailed breakdown of our alignment approach and outcomes using an RCC–5 logic reasoner toolkit (Chen et al. 2014) is provided in the **Supplemental Information, SI1 to SI4**. For further information, see also Jansen & Franz (2015), Franz et al. (2016a,b).

### Species distribution modeling

We used the modeling program Maxent, Version 3.4, to generate habitat models for the species of *Minyomerus* [JF2018] (Figs. 4–7) based on documented occurrence records (Phillips et al. 2004, 2006, Elith et al. 2011). The default settings were adjusted to Max number background points = 100,000 and Iterations = 10. Cross-validation was used to leverage all available locality data; however, no models could be created for species with two or fewer documented localities. We selected 19 bioclimatic variables and elevation as Environmental Layers in Maxent, obtained from WorldClim (Hijmans et al. 2005). The layers were downloaded by tile (zones 11–13 and 21–23), with a 30 arc-second resolution (projected using WSG 84) to provide adequate coverage of the full distribution of the genus. Layerwise assembly of tiles was done using QGIS, Version 2.18.16 ‘Las Palmas’, creating composite maps of six tiles each to use in species distribution modeling (Quantum GIS Development Team 2018).

The rasterized predictive probabilities were imported into QGIS, where each file was designated a specific color. Each pixel in the raster was assigned a linearly interpolated saturation of that color, with increasing saturation denoting an increased probability of successful prediction of species presence at that point. Pixels with a value below 0.50 were rendered transparent so that the maps only show regions with a greater than 50% chance of successful prediction. The raster files were clipped to remove extraneous predicted regions based on: (1) predictive probability (i.e., removing large areas with only transparent pixels) and (2) geographic extent (accounting for endemicity). For example, a species endemic to the Snake River Valley of Idaho does not require a predictive model for bioclimatically similar habitats in the Chihuahuan Desert. Documented occurrence records are laid over the modeled habitat ranges as colored circles on their respective maps (Figs. 4–7), along with vector layers of country (white) and state (gray) borders (Hijmans et al. 2012).

229 **Nomenclature**

230 The electronic version of this article in Portable Document Format (PDF) will represent a published work  
231 according to the International Commission on Zoological Nomenclature (ICZN), and hence the new names  
232 contained in the electronic version are effectively published under that Code from the electronic edition  
233 alone. This published work and the nomenclatural acts it contains have been registered in ZooBank, the  
234 online registration system for the ICZN. The ZooBank LSIDs (Life Science Identifiers) can be resolved  
235 and the associated information viewed through any standard web browser by appending the LSID to  
236 the prefix <http://zoobank.org/>. The LSID for this publication is: urn:lsid:zoobank.org:pub:0AEE5733-  
237 06D1-401F-88C9-0D5232FBFC7A. The online version of this work is archived and available from the  
238 following digital repositories: PeerJ, PubMed Central and CLOCKSS.

239 Minyomerus ampullaceus: Minyomerus franko: Minyomerus sculptilis: Minyomerus tylotos:

240 **DESCRIPTIONS OF NEW SPECIES**

241 ***Minyomerus ampullaceus* Jansen & Franz sec. Jansen & Franz, 2018; sp. n.**

242 urn:lsid:zoobank.org:act:24943E17-F20E-4E3C-A3A1-A1D4D907B48E

243 Figures 8-13

244 **Diagnosis**

245 *Minyomerus ampullaceus* [JF2018] is best differentiated from other congeners by its unique body shape,  
246 which most prominently features a strongly constricted, sub-cylindrical pronotum and greatly protuberant  
247 elytra; this combination gives the species a distinctly flask- or bottle-shaped appearance. Due to the  
248 relatively poor condition of the scales and setae of the holotype, color and setation cannot be reliably  
249 used for identification. However, the elytra themselves are unique in shape, and diagnostic, together  
250 nearly 2× the width of the pronotum at their widest point, and nearly 3/4× as wide as long in dorsal  
251 view. In lateral view the anterior and posterior declivities of the elytra are strongly abrupt, and nearly  
252 vertical; most notably, the anterior margin of the elytra projects strongly and characteristically dorsad of  
253 its articulation with the posterior pronotal margin. The spermatheca is also quite distinct, having a highly  
254 elongate projection of the corpus aligned with midline of the ramus, which is basally tapered and angled  
255 at nearly 45° to the corpus.

256 **Description of female**

257 **Habitus** Length 3.76 mm, width 1.76 mm, length/width ratio 2.14, widest at anterior 1/3 of elytra.  
258 Integument orange-brown to black. Scales with variously interspersed colors ranging from slightly  
259 off-white to beige to yellow. Setae recumbent to sub-recumbent, white to brown in color.

260 **Mandibles** Partially covered with white, slightly opalescent scales, with 3 longer setae, and 1 shorter  
261 seta between these.

262 **Rostrum** Length 0.54 mm, anterior portion 1.5-2× broader than long, rostrum/pronotum length ratio  
263 0.57, rostrum length/width ratio 1.10. Separation of rostrum from head generally obscure. Dorsal outline  
264 of rostrum nearly square, anterior half of dorsal surface mesally concave, posterior half coarsely but  
265 shallowly punctate to rugose. Rostrum in lateral view nearly square; apical margin broadly bisinuate and  
266 emarginate, with 2 pairs of large vibrissae. Nasal plate defined by Y-shaped, impressed lines, convex,  
267 integument partially covered with white scales. Margins of mandibular incision directed ca. 15° outward  
268 dorsally in frontal view. Ventrolateral sulci strongly defined, beginning as a narrow sulcus posteriad of  
269 insertion point of mandibles, running parallel to scrobe, terminating in a ventral fovea.

270 **Antennae** Small tooth formed by overhanging dorsal margin of scrobe directly ventrad of margin of  
271 eye. Scape extending to posterior 1/3 of eye. Funicular segments V-VII and club missing.

272 **Head** Eyes globular, anterodorsal margin of each eye feebly impressed, posterior margin elevated  
273 from lateral surface of head; eyes separated in dorsal view by 4× their anterior-posterior length, set off  
274 from anterior prothoracic margin by 1/3 of their anterior-posterior length. Head without any transverse  
275 post-ocular impression.

276 **Pronotum** Length/width ratio 0.88; widest near midpoint. Anterior margin slightly arcuate, lateral  
277 margins curved and widening into a bulge just anteriad of midpoint of pronotum, posterior margin straight,  
278 with a slight mesal incurvature. Pronotum in lateral view with setae that reach beyond anterior margin by  
279 1/2 of their length; these setae becoming evenly longer and more erect laterally, reaching a maximum  
280 length equal to 1/2 of length of eye. Anterolateral margin with a reduced tuft of 6-7 post-ocular vibrissae  
281 present, emerging near ventral 1/2 of eye, and stopping just below ventral margin of eye; vibrissae sub-  
282 equal in length at 1/3 of anterior-posterior length of eye, except for three vibrissae achieving a maximum  
283 length similar to anterior-posterior length of eye.

284 **Scutellum** Exposed, margins straight.

285 **Pleurites** Metepisternum hidden by elytron.

286 **Thoracic sterna** Mesocoxal cavities separated by 1/4× width of mesocoxal cavity. Metasternum with  
287 transverse sulcus not apparent; metacoxal cavities widely separated by ca. 2× their width.

288 **Legs** Profemur/pronotum length ratio 1.04; profemur with distal 1/5 produced ventrally as a rounded  
289 projection covering tibial joint; condyle of tibial articulation occupying 4/5 of distal surface and 1/5  
290 length of femur. Protibia/profemur length ratio 0.93; protibial apex with ventral setal comb recessed in  
291 an incurved groove; mucro present as a large, black, sub-triangular, medially-projected tooth, which is  
292 approximately equilateral and whose sides are sub-equal in length to surrounding setae. Protarsus with  
293 tarsomere III 1.25× as long as II; wider than long. Metatibial apex with almond shaped convexity ringed  
294 by 10 short, spiniform setae.

295 **Elytra** Length/width ratio 2.66; widest at anterior 1/3; anterior margins jointly almost 2× wider than  
296 posterior margin of pronotum and strongly produced dorsally from margin of pronotum; lateral margins  
297 evenly rounded until posterior 1/3, more strongly rounded and converging thereafter. Posterior declivity  
298 angled at nearly 85° to main body axis. Elytra with 10 complete striae; striae shallow; punctures faint  
299 beneath appressed scales, separated by 5-7× their diameter; intervals very slightly elevated.

300 **Abdominal sterna** Ventrite III anteromesally incurved around a fovea located mesally on anterior  
301 margin, posterior margin elevated and set off from IV along lateral 1/3s of its length. Sternum VII mesally  
302 1/2× as long as wide; anterior margin weakly curved.

303 **Tergum** Pygidium (tergum VIII) sub-conical; posterior margin emarginate; medial 1/3 of anterior 3/5  
304 of pygidium less sclerotized.

305 **Sternum VIII** Anterior laminar edges each incurved forming a 115° angle with lateral margin, this angle  
306 distinctly sclerotized; posterior 1/2 of lamina porose throughout, laminar arms more sclerotized medially;  
307 posterior edge evenly, moderately arcuate.

308 **Ovipositor** Coxites in dorsal view slightly longer than broad, with a medial region that is weakly  
309 sclerotized.

310 **Spermatheca** Comma-shaped; collum expanded to form a long, cylindrical projection, sub-equal in  
311 length to ramus, 1/3× width of corpus, angled at 45° to corpus, apically with a reduced hood-shaped  
312 projection; ramus elongate, bulbous, slightly wider than thickness of corpus, basally constricted to form a  
313 short stalk; corpus not greatly swollen; cornu sub-equal in length to corpus and collum, recurved distally  
314 to form an inner angle of 60° to corpus, straight and gradually narrowing along basal 2/3, with apical 1/3  
315 abruptly narrowed, angled at 45° to corpus, and tapering to a slight knob.

316 **Description of male**

317 Male not available or known.

318 **Comments**

319 Due to the limited number of specimens of this species, dissections of mouthparts could not be performed.

320 **Etymology**

321 Named in reference to the shape of the body in dorsal view, which appears bottle-shaped due to the large  
322 elytra and comparatively cylindrical pronotum – *ampullaceus* = "flasklike"; Latin adjective (Brown 1956).

323 **Material examined**

324 **Holotype** ♀ “Carlsbad, N.M.; Geococcyx calif; 144640” (USNM).

325 **Distribution**

326 This species is known only from Carlsbad, New Mexico (USA), from an unspecified locality; the location  
327 of the city is shown in Fig. 5.

328 **Natural history**

329 No host plant associations have been documented. The label indicates “Geococcyx calif”; this is  
330 presumably a reference to *Geococcyx californianus* (Lesson, 1829) [non-focal] (Cuculidae [non-focal]),  
331 the Greater Roadrunner. We had initially believed that this indicated a specimen found in a roadrunner  
332 nest; however, according to our reviewers, the USNM frequently assisted with the identification of insect  
333 specimens retrieved from the stomach contents of birds, and thus the specimen was most likely retrieved  
334 from the gut contents of a roadrunner. This seems quite likely given the poor external condition of the  
335 specimen. It is unknown whether this species is parthenogenetic.

336 ***Minyomerus franko* Jansen & Franz sec. Jansen & Franz, 2018; sp. n.**

337 urn:lsid:zoobank.org:act:F8C0153E-DF0E-40E0-AF31-EBEA7075D06D

338 Figures 14-22

339 **Diagnosis**

340 *Minyomerus franko* [JF2018] is readily distinguished from other congeners by the strikingly long setae  
341 of the anterior margin of the pronotum, which project laterally up to 80° from the longitudinal axis of  
342 the body and achieve a maximum length at least equaling the diameter of the eye. In addition, the setae  
343 lining the dorsal margin of the ocular impression are elongate and reach a length equal to 1/2 - 3/4 × the  
344 diameter of the eye. The spermatheca has a short, somewhat bulbous corpus, with the ramus sub-equal  
345 in size and perpendicular to the corpus, and the collum is strongly recurved along the basal 1/3 of its  
346 length. The aedeagus is relatively short and wide, and is abruptly constricted in the apical 1/5 of its length,  
347 thereafter tapered to a rounded point.

348 **Description of female**

349 **Habitus** Length 3.10-3.30 mm, width 1.38-1.44 mm, length/width ratio 2.25-2.29, widest at anterior  
350 1/3-1/4 of elytra. Integument orange-brown to black. Scales with variously interspersed colors ranging  
351 from slightly off-white or beige to manila/tan to dark coffee brown, in some specimens appearing semi-  
352 translucent (in others opaque). Setae linear to slightly apically explanate, appearing minutely spatulate,  
353 sub-recumbent to sub-erect, white or brown in color.

354 **Mandibles** Covered with white scales, with 3 longer setae, and 1-2 shorter setae between these.

355 **Maxillae** Cardo bifurcate at base with an inner angle typically between 90–120°, arms of equal length,  
356 inner (mesal) arm nearly 1.5× thicker than outer arm, both arms of bifurcation equal in length to apically  
357 outcurved arm, glabrous. Stipes sub-quadrata, roughly equal in length to each bifurcation of cardo, with a  
358 single lateral seta. Galeo-lacinial complex nearly extending to apex of maxillary palpomere II; complex  
359 mesally membranous, laterally sclerotized, with sharp demarcation of sclerotized region separating  
360 palpiger from galeo-lacinial complex; setose in membranous area just adjacent to sclerotized region, setae  
361 covering 2/3 of dorsal surface area; dorsally with 7 apicomosal lacinial teeth; ventrally with 4 reduced  
362 lacinial teeth. Palpiger with a single lateral seta, otherwise glabrous and evenly sclerotized throughout.

363 **Maxillary palps** I apically oblique, apical end forming a 45° angle with base, with 2 apical setae; II  
364 sub-cylindrical, with 1 apical seta.

365 **Labium** Prementum roughly trapezoidal; apical margins angulate, ventral margin gently sinuate, dorsal  
366 margin straight; lateral margins feebly incurved near posterior margin; basal margin arcuate. Labial palps  
367 3-segmented, I with apical 2/3 projecting beyond margin of prementum, exceeding apex of ligula; III  
368 slightly longer than II.

369 **Rostrum** Length 0.46-0.48 mm, anterior portion 1.75-2.25× broader than long, rostrum/pronotum  
370 length ratio 0.58-0.59, rostrum length/width ratio 1.21-1.26. Separation of rostrum from head generally  
371 obscure. Dorsal outline of rostrum sub-rectangular, anterior half of dorsal surface feebly impressed,  
372 posterior half coarsely but shallowly punctate to rugose. Rostrum in lateral view nearly square; apical  
373 margin bisinuate and emarginate, with 2 large vibrissae. Nasal plate defined by broad, V-shaped, shallowly  
374 impressed lines, anteromesally slightly convex, integument partially covered with white scales. Margins  
375 of mandibular incision directed ca. 15° outward dorsally in frontal view. Ventrolateral sulci weakly  
376 defined (or entirely absent in some specimens) as a broad concavity dorsad of insertion point of mandibles,  
377 running parallel to scrobe, becoming flatter posteriorly and disappearing ventrally. Dorsal surface of  
378 rostrum with short, linear, median fovea. Rostrum ventrally lacking sulci at corners of oral cavity.

379 **Antennae** Small tooth formed by overhanging dorsal margin of scrobe anterior to margin of eye by 1/5  
380 of length of eye. Scape nearly extending to posterior 1/4 of eye. Terminal funicular antennomere lacking  
381 appressed scales, having instead a covering of apically-directed pubescence with interspersed sub-erect  
382 setae. Club nearly 3× as long as wide.

383 **Head** Eyes globular to slightly elongate, slanted ca. 35° antero-ventrally; eyes separated in dorsal  
384 view by 4× their anterior-posterior length, set off from anterior prothoracic margin by 1/3 of their  
385 anterior-posterior length. Head without any transverse post-ocular impression.

386 **Pronotum** Length/width ratio 0.84-0.86; widest near anterior 1/3, between anterior constriction and  
387 midpoint. Anterior margin arcuate, lateral margins curved and widening into a slight bulge just anteriad  
388 of midpoint of pronotum, posterior margin straight, with a slight mesal incurvature. Pronotum in lateral  
389 view with setae that reach just beyond anterior margin, angled laterally at 45-80° to longitudinal axis, and  
390 strikingly long; these setae becoming evenly longer and more angled laterally, reaching a maximum length  
391 nearly equal to length of eye. Anterolateral margin with a reduced tuft of 5 post-ocular vibrissae present,  
392 emerging near ventral 1/2 of eye, and stopping just below ventral margin of eye; vibrissae sub-equal  
393 in length at 1/3× anterior-posterior length of eye, except for one vibrissa achieving a maximum length  
394 similar to anterior-posterior length of eye.

395 **Scutellum** Narrowly exposed, with visible area approximately equal to length of appressed scales,  
396 margins straight.

397 **Pleurites** Metepisternum nearly hidden by elytron except for triangular extension.

398 **Thoracic sterna** Mesocoxal cavities separated by 1/3× width of mesocoxal cavity. Metasternum with  
399 transverse sulcus not apparent; metacoxal cavities widely separated by ca. 2× their width.

400 **Legs** Profemur/pronotum length ratio 1.01-1.02; profemur with distal 1/5 produced ventrally as a sub-  
401 rectangular projection covering tibial joint; condyle of tibial articulation occupying 4/5 of distal surface  
402 and 1/5 length of femur. Protibia/profemur length ratio 0.86-0.89; protibial apex with ventral setal comb  
403 recessed in a subtly incurved groove; mucro present as a large, black, sub-triangular, medially-projected  
404 tooth, which is approximately equilateral and whose sides are sub-equal in length to surrounding setae.  
405 Protarsus with tarsomere III 2× as long as II; wider than long. Metatibial apex with almond shaped  
406 convexity ringed by 8-9 short, spiniform setae.

407 **Elytra** Length/width ratio 3.08-3.20; widest at anterior 1/3-1/4; anterior margins jointly 1.5× wider than  
408 posterior margin of pronotum; lateral margins sub-parallel to slightly rounded after anterior 1/3, more  
409 strongly rounded and converging in posterior 1/3. Posterior declivity angled at 70-85° to main body axis.  
410 Elytra with 10 complete striae; striae shallow; punctures faint beneath appressed scales, separated by  
411 5-7× their diameter; intervals very slightly elevated.

412 **Abdominal sterna** Ventrite III anteromesally incurved around a fovea located mesally on anterior  
413 margin, posterior margin elevated and set off from IV along lateral 1/3s of its length. Sternum VII mesally  
414 1/2× as long as wide; setae darkening, lengthening, and becoming more erect in posterior 2/3; anterior  
415 margin weakly curved.

416 **Tergum** Pygidium (tergum VIII) sub-cylindrical; medial 1/3 of anterior 2/3 of pygidium less sclerotized.

417 **Sternum VIII** Anterior laminar edges each incurved forming a 140° angle with lateral margin; slightly  
418 less sclerotized medially between arms of bifurcation; posterior edge subtly incurved medially.

419 **Ovipositor** Coxites 1.5× as long as broad, glabrous; styli 1/2× as long as coxites. Genital chamber  
420 apically sclerotized.

421 **Spermatheca** Comma-shaped; column short, apically with a large, hood-shaped projection angled  
422 at ca. 60° to ramus, nearly equal in length and contiously aligned with curvature of bulb of ramus;  
423 collum sub-contiguous with, and angled at 90° to ramus; ramus elongate, sub-cylindrical to slightly  
424 bulbous, 4/5× thickness of corpus; corpus swollen, 1.25× thicknes of ramus and 1.5× thickness of cornu;  
425 cornu elongate, strongly recurved in basal 1/3, nearly straight thereafter and narrowing apically, abruptly  
426 narrowed in apical 1/3 with apex angled at 30° to corpus.

427 **Description of male**

428 Similar to female, except where noted.

429 **Habitus** Length 2.47-2.81 mm, width 0.99-1.24 mm, length/width ratio 2.27-2.49. Rostrum length  
430 0.30-0.42 mm, rostrum/pronotum length ratio 0.44-0.53, rostrum length/width ratio 1.00-1.08. Pronotum  
431 length/width ratio 0.91-1.00. Profemur/pronotum length ratio 0.87-0.90, protibia/profemur length ratio  
432 0.87-0.97. Elytra length/width ratio 3.00-3.10.

433 **Elytra** Elytral declivity more angulate than female on average, forming an 80° angle to main body axis,  
434 but otherwise as in female.

435 **Abdominal sterna** S sternum VII 2/5-1/2× as long as wide, posterior margin arcuate mesally.

436 **Tergum** Pygidium (tergum VIII) with posterior 1/3 punctate; anterior 2/3 rugose.

437 **Sternum IX** Spiculum gastrale 2× length of aedeagal pedon. Laminar alae located on lateral 1/4 of  
438 posterior margin.

439 **Aedeagus** Length/width ratio 2.78-3.16; lateral margins very slightly converging posteriorly, abruptly  
440 constricted and more strongly converging in apical 1/5. Pedon in lateral view becoming gradually narrower  
441 posteriorly in anterior 1/2, ventral margins in posterior 1/2 abruptly curving to meet dorsal margins at a  
442 rounded apical point. Flagellum with large, elonage, tortuous apical sclerite, sclerite nearly as long as  
443 pedon, with complex, asymmetrical interior structure.

444 **Etymology**

445 Named in reference to the long, somewhat unkempt, erect setae on the anterior margin of the pronotum—  
446 *franko* = "free"; Old High-German adjective (Brown 1956).

447 **Material examined**

448 **Holotype** ♀ "MEX: S.L.P 1 km N.; Entronque El Huizache; 1493 m 2.VI.87; R. Anderson, *Sphaeralcea*;  
449 *hastula* A. Gray" [non-focal] (**CMNC**).

450 **Paratypes** Same label information as female holotype (**CMNC**: 1 ♀, 1 ♂; **TAMU**: 2 ♂); "MEXICO: S.L.P;  
451 19.6 mi. n. Huizache; July 25, 1976; Peigler, Gruetzmacher, R&M Murray, Schaffner" (**CMNC**: 1 ♂);  
452 "MEXICO: San Luis Potosí; Entronque el Hulzache; 2 June 1987; R. Turnbow" (**USNM**: 1 ♀; **CMNC**: 1 ♂);  
453 "MEXICO: Tamaulipas; 8.8 mi. ne. Jaumave; October 10, 1973; Gaumer & Clark" (**TAMU**: 2♀); "9 mi  
454 east Santo Domingo, S.L.P.; Mexico XI-14-68; Veryl V. Board" (**TAMU**: 2 ♂).

455 **Distribution**

456 This species has been found in San Luis Potosí and Tamaulipas (Mexico). It is likely to be found  
457 throughout the Chihuahuan Desert and arid regions of south-central Mexico based on habitat similarity  
458 (Fig. 6).

459 **Natural history**

460 Associated with spear globemallow *Sphaeralcea hastulata* A. Gray [non-focal] (Malvaceae [non-focal]).  
461 The indication of "Sphaeralcea hastula A. Gray" is not a valid name and appears to be a misspelling of  
462 *Sphaeralcea hastulata* [non-focal].

463 **Minyomerus sculptilis Jansen & Franz sec. Jansen & Franz, 2018; sp. n.**

464 urn:lsid:zoobank.org:act:EA0B1AD9-68F2-4409-A0F8-903B0DA0FFF9

465 Figures 23-29

466 **Diagnosis**

467 *Minyomerus sculptilis* [JF2018] is best distinguished from other congeners, especially *Minyomerus*  
468 *imberbus* Jansen & Franz, 2015 [JF2015], by a combination of characters, as follows. The interspersed  
469 setae on the body are linear and either brown or white. The anterior margin of the pronotum bears a  
470 reduced tuft of post-ocular vibrissae. The head is barely elevated between the eyes. The ventrolateral  
471 sulci of the rostrum are well defined. The lateral face of each elytron has the intervals raised and well  
472 sculpted in appearance. The spermatheca is distinct and has an elongate, annulate, basally tapered ramus,  
473 which is slightly thinner than corpus. The cornu is strongly recurved in the basal half, giving it a uniquely  
474 sinuate appearance. Both the corpus and cornu terminate in large, hood-shaped, explanate projections  
475 equal in size to the ramus. The aedeagus is elongate, acutely angulate, and narrowing towards the apex  
476 more strongly in the region of the ostium.

477 **Description of female**

478 **Habitus** Length 3.39-3.70 mm, width 1.33-1.58 mm, length/width ratio 2.34-2.55, widest at anterior  
479 1/5 of elytra. Integument orange-brown to black. Scales with variously interspersed colors ranging from  
480 slightly off-white or beige to golden brown to dark coffee brown. Setae sub-recumbent to sub-erect, white  
481 to brown in color.

482 **Mandibles** Covered with white scales, with 3 longer setae, and 1 shorter seta between these.

483 **Rostrum** Length 0.50-0.59 mm, anterior portion ca. 1.5× broader than long, rostrum/pronotum length  
484 ratio 0.66-0.67, rostrum length/width ratio 1.43-1.48. Separation of rostrum from head generally obscure.  
485 Dorsal outline of rostrum nearly square, anterior half of dorsal surface mesally concave, posterior half  
486 coarsely but shallowly punctate to rugose. Rostrum in lateral view nearly square; apical margin bisinuate  
487 and emarginate, with 2 pairs of large vibrissae. Nasal plate defined by Y-shaped, impressed lines, convex,  
488 integument covered with white scales. Margins of mandibular incision directed ca. 15-20° outward  
489 dorsally in frontal view. Ventrolateral sulci strongly defined, beginning as a narrow sulcus posteriad of  
490 insertion point of mandibles, running parallel to scrobe, terminating in a ventral fovea.

491 **Antennae** Dorsal margin of scrobe overhanging broadly (not forming a minute tooth). Funicle slightly  
492 longer than scape. Scape extending to posterior 1/4 of eye. Club nearly 3× as long as wide.

493 **Head** Eyes globular, anterodorsal margin of each eye impressed, posterior margin slightly elevated  
494 from lateral surface of head; eyes separated in dorsal view by 5× their anterior-posterior length, set off  
495 from anterior prothoracic margin by 1/4 of their anterior-posterior length. Head between eyes rugose and  
496 slightly bulging.

497 **Pronotum** Length/width ratio 0.85-0.87; widest near anterior 2/5. Anterior margin arcuate, subtly  
498 incurved mesally, and somewhat produced dorsally; anterior constriction broad, posterior margin slightly  
499 arcuate. Pronotum in lateral view with setae that reach beyond anterior margin; these setae becoming  
500 slightly longer and more erect laterally. Anterolateral margin with a reduced tuft of 3-6 post-ocular  
501 vibrissae present, emerging near ventral 1/2 of eye, and stopping just below ventral margin of eye;  
502 vibrissae varying in length from 1/2× anterior-posterior length of eye to a maximum length similar to  
503 anterior-posterior length of eye.

504 **Scutellum** Exposed, margins straight.

505 **Pleurites** Metepisternum nearly hidden by elytron except for triangular extension.

506 **Thoracic sterna** Mesocoxal cavities separated by 1/3× width of mesocoxal cavity. Metasternum with  
507 transverse sulcus not apparent; metacoxal cavities widely separated by ca. 2× their width.

508 **Legs** Profemur/pronotum length ratio 0.92-1.03; profemur with distal 1/6 produced ventrally as a  
509 slightly rounded, sub-rectangular projection covering tibial joint; condyle of tibial articulation occupying  
510 4/5 of distal surface and 1/6 length of femur. Protibia/profemur length ratio 0.87-0.93; protibial apex with  
511 ventral setal comb recessed in a subtly incurved groove; mucro not apparent. Protarsus with tarsomere III  
512 1.5× as long as II; wider than long. Metatibial apex with almond shaped convexity ringed by 10-12 short,  
513 spiniform setae.

514   **Elytra** Length/width ratio 3.12-3.16; widest at anterior 1/5; anterior margins jointly 1.5-2× wider  
515 than posterior margin of pronotum; lateral margins gently converging after anterior 1/5, more strongly  
516 converging in posterior 1/4. Posterior declivity angled at 65-70° to main body axis. Elytra with 10  
517 complete striae; striae broadly sculpted; punctures faint beneath appressed scales, separated by 5-7× their  
518 diameter; intervals elevated, with every second interval, beginning at elytral suture, more strongly raised  
519 than adjacent intervals.

520   **Abdominal sterna** Ventrite III anteromesally incurved around a fovea located mesally on anterior  
521 margin, posterior margin elevated and set off from IV along lateral 1/3s of its length. Sternum VII mesally  
522 2/3× as long as wide; anterior margin straight.

523   **Tergum** Pygidium sub-cylindrical; medial 1/2 of anterior 3/5 of pygidium less sclerotized.

524   **Sternum VIII** Anterior laminar edges of spiculum ventrale each incurved forming a 125° angle with  
525 lateral margin; lamina more sclerotized medially; posterior margin medially incurved.

526   **Ovipositor** Coxites as long as broad; styli as long as coxites, glabrous.

527   **Spermatheca** S-shaped; collum short, apically with a large, hood-shaped projection roughly aligned  
528 with central axis of corpus, nearly equal in length to bulb of ramus; collum sub-contiguous with, and  
529 angled at 30° to ramus; ramus elongate, sub-cylindrical to slightly bulbous, 3/4× thickness of corpus,  
530 with a short stalk oriented at ca. 45° to the corpus; corpus swollen, 1.3× thickness of ramus; cornu short,  
531 2.5-3× length of ramus, recurved and strongly arched in basal 1/2, forming an inner angle of ca. 80°,  
532 feebly sinuate thereafter, with apical 1/2 expanded, then abruptly constricted near apical 1/4 to a fine  
533 point.

534   **Description of male**

535 Similar to female, except where noted.

536   **Habitus** Length 3.10 mm, width 1.22 mm, length/width ratio 2.54. Rostrum length 0.53 mm, rostrum/pronotum length ratio 0.65, rostrum length/width ratio 1.66. Pronotum length/width ratio 0.99.  
537 Profemur/pronotum length ratio 1.01, protibia/profemur length ratio 0.82. Elytra length/width ratio 3.18.  
538

539   **Elytra** Elytral declivity slightly less angulate than female, forming a 60° angle to main body axis, but  
540 otherwise as in female.

541   **Abdominal sterna** Sternum VII 1/2× as long as wide, posterior margin feebly arcuate mesally.

542   **Tergum** Pygidium (tergum VIII) with mesal 1/3 of posterior margin subtly incurved; posterior 2/3  
543 punctate; anterior 1/3 rugose.

544   **Sternum VIII** Consisting of 2 sub-triangular sclerites; antero-laterally with a sharply-pointed projection  
545 as long as anterior-posterior length of triangular portion of sclerite.

546   **Aedeagus** Length/width ratio 7.00; lateral margins parallel, more strongly converging in region of  
547 ostium. In lateral view, width of pedon even throughout in anterior 2/3, ventral margins in posterior 1/3  
548 becoming straight towards apex, then curving to meet dorsal margins at a sharp apical point; apex acutely  
549 angulate. Flagellum without apparent sclerite.

550   **Comments**

551 Due to the limited number of specimens of this species, dissections of mouthparts could not be performed.

552   **Etymology**

553 Named in reference to the elevated elytral intervals, which give this species a sculpted appearance –  
554 *sculptilis* = “sculpted”; Latin adjective (Brown 1956).

555   **Material examined**

556   **Holotype** ♀ “Burley, Idaho; #7, 5-20-32; A.[rtemisia] tridentata [non-focal]; David E. Fox” (**USNM**).

557   **Paratypes** “Milner, Idaho; #5a, 7-9-31; S.[alsola] pestifer; David E. Fox” (**CMNC**: 1 ♀); “Hazelton, Ida;  
558 #10 4/29/30; N.[orta] altissima” (**USNM**: 1 ♂)

559 **Distribution**

560 This species has been found in three localities along the Snake River in Idaho (USA), and is thought to be  
561 endemic to the Snake River Plain (Fig. 7).

562 **Natural history**

563 Associated with big sagebrush *Artemisia tridentata* Nutt. [non-focal] (Asteraceae [non-focal]), tumble-  
564 weed *Salsola tragus* L. [non-focal] (= *Salsola pestifer* A. Nelson [non-focal]) (Amaranthaceae [non-focal]),  
565 and tall tumblemustard *Sisymbrium altissimum* L. [non-focal] (= *Norta altissima* (L.) Britt. [non-focal])  
566 (Brassicaceae [non-focal]).

567 ***Minyomerus tylotos* Jansen & Franz sec. Jansen & Franz, 2018; sp. n.**

568 urn:lsid:zoobank.org:act:10CD3562-5969-4BCF-ACFE-BB0E5E2BF9A6

569 Figures 30-36

570 **Diagnosis**

571 *Minyomerus tylotos* [JF2018] is most readily distinguished from other congeners by a combination  
572 of characters, as follows. The nasal plate lacks distinct impressions, having instead a poorly defined  
573 anteromesal convexity completely and evenly covered with white scales. The frons is protuberant and  
574 moderately punctate. The entire body, including the legs, head, and venter, are clothed with brown,  
575 linear to minutely apically expanded setae, which are of similar length throughout and appear distinctly  
576 undifferentiated and uniform across body regions. The body is somewhat bulky, with the pronotum  
577 protuberant laterally and globular in dorsal view. The setae lining the anterodorsal margin of the pronotum  
578 uniquely apically explanate, with a longitudinal, medial, ridge-like portion that tapers to either side  
579 apicolaterally (visible at high magnification). The lateral margins of the elytra are protuberant anteriorly  
580 and sub-parallel along the between anterior 1/5 and posterior 1/3 of their length. The spermatheca has the  
581 corpus narrow throughout, equal in thickness to the collum. The ramus is basally stalked and apically  
582 bulbous. The collum exhibits a double-bend, and is recurved.

583 **Description of female**

584 **Habitus** Length 3.46-3.62 mm, width 1.42-1.54 mm, length/width ratio 2.35-2.44, widest at anterior  
585 1/6 of elytra. Integument orange-brown to black. Scales with variously interspersed colors ranging  
586 from slightly off-white or beige to manila/tan to dark coffee brown, in some specimens appearing  
587 semi-translucent (in others opaque). Setae linear to apically explanate, appearing minutely spatulate,  
588 sub-recumbent to sub-erect, tan to brown in color.

589 **Mandibles** Covered with white scales, with 2-3 longer setae, and 1-3 shorter setae between these.

590 **Maxillae** Cardo bifurcate at base with an inner angle of ca. 90°, arms roughly equal in length and  
591 width, arms of bifurcation equal in length to apically outcurved arm. Stipes sub-rectangular, 1.5× wider  
592 than long, roughly equal in width to inner arm of bifurcation of cardo, glabrous. Galeo-lacinial complex  
593 nearly extending to apex of maxillary palpomere I; complex mesally membranous, laterally sclerotized,  
594 with sharp demarcation of sclerotized region separating palpiger from galeo-lacinial complex; setose in  
595 membranous area just adjacent to sclerotized region, setae covering 1/2 of dorsal surface area; dorsally  
596 with 5 apicomosal lacinial teeth; ventrally with 3 reduced lacinial teeth. Palpiger with a single lateral seta,  
597 otherwise glabrous, anterior 1/2 membranous, posteriorly sclerotized.

598 **Maxillary palps** I apically oblique, apical end forming a 45° angle with base, with 2 apical setae; II  
599 sub-cylindrical, with 1 apical seta.

600 **Labium** Prementum roughly pentagonal; apical margins arcuate, medially angulate; lateral margins  
601 feebly incurved; basal margin arcuate. Labial palps 3-segmented, I with apical 1/2 projecting beyond  
602 margin of prementum, reaching apex of ligula; III slightly longer than II.

603 **Rostrum** Length 0.49-0.50 mm, anterior portion 2.25-2.5× broader than long, rostrum/pronotum length  
604 ratio 0.58-0.62, rostrum length/width ratio 1.26-1.32. Separation of rostrum from head generally obscure.  
605 Dorsal outline of rostrum nearly square, anterior half of dorsal surface feebly impressed, posterior half  
606 coarsely but shallowly punctate to rugose. Rostrum in lateral view nearly square; apical margin strongly  
607 bisinuate and emarginate, appearing medially notched, with 2 large vibrissae. Nasal plate lacking distinct  
608 impressions, having instead a poorly defined anteromesal convexity, integument completely and evenly

609 covered with white scales. Margins of mandibular incision directed ca. 25-30° outward dorsally in frontal  
610 view. Ventrolateral sulci weakly defined as a broad concavity dorsad of insertion point of mandibles,  
611 running parallel to scrobe, becoming flatter posteriorly and disappearing ventrally. Dorsal surface of  
612 rostrum with median fovea short and linear, or punctate. Rostrum ventrally with sub-parallel sulci  
613 beginning at corners of oral cavity and continuing halfway to back of head.

614 **Antennae** Minute tooth formed by overhanging dorsal margin of scrobe anterior to margin of eye by  
615 1/3 of length of eye. Scape extending to posterior margin of eye. Terminal funicular antennomere lacking  
616 appressed scales, having instead a covering of apically-directed pubescence with interspersed sub-erect  
617 setae. Club nearly 3× as long as wide.

618 **Head** Eyes globular and somewhat elongate, strongly impressed, slanted ca. 45° antero-ventrally; eyes  
619 separated in dorsal view by 4× their anterior-posterior length, set off from anterior prothoracic margin by  
620 1/4 of their anterior-posterior length. Head between eyes punctate and protuberant.

621 **Pronotum** Length/width ratio 0.88-0.89; widest near anterior 2/5; somewhat globular. Anterior margin  
622 arcuate, but feebly incurved mesally, lateral margins evenly curved and widening into a bulge just anteriad  
623 of midpoint of pronotum, posterior margin straight, with a slight mesal incurvature. Pronotum in lateral  
624 view with transverse ventrolateral sulci strongly excavated and distinctly sculptured; with short, recumbent  
625 to sub-erect setae that barely attain or reach just beyond anterior margin; these setae becoming shorter  
626 and more erect laterally, reaching a maximum length nearly equal to length of eye; dorsally, these setae  
627 become uniquely apically explanate, with a longitudinal, medial, ridge-like portion that tapers to either  
628 side apicolaterally. Anterolateral margin with a single ocular vibrissa present, emerging near ventral  
629 margin of eye; vibrissa achieving a maximum length of 2/5 of anterior-posterior length of eye.

630 **Scutellum** Not exposed.

631 **Pleurites** Metepisternum nearly hidden by elytron except for triangular extension.

632 **Thoracic sterna** Mesocoxal cavities separated by 1/3× width of mesocoxal cavity. Metasternum with  
633 transverse sulcus not apparent; metacoxal cavities widely separated by ca. 3× their width.

634 **Legs** Profemur/pronotum length ratio 0.90-0.96; profemur with distal 1/5 produced ventrally as a  
635 sub-rectangular projection covering tibial joint; condyle of tibial articulation occupying 4/5 of distal  
636 surface and 1/5 length of femur. Protibia/profemur length ratio 0.86-0.91; protibial apex with ventral setal  
637 comb recessed in a subtly incurved groove; mucro present as an acute, medially-projected tooth, which is  
638 approximately equal in length to surrounding setae. Protarsus with tarsomere III 2× as long as II; wider  
639 than long. Metatibial apex with weakly projecting, poorly defined, narrow convexity laterally flanged by  
640 5 short, spiniform setae.

641 **Elytra** Length/width ratio 3.03-3.21; widest at anterior 1/6; anterior margins jointly 1.5-2× wider  
642 than posterior margin of pronotum; lateral margins nearly straight and sub-parallel after anterior 1/5,  
643 converging in posterior 1/3. Posterior declivity angled at 70-75° to main body axis. Elytra with 10  
644 complete striae; striae broadly sculpted; punctures broad and faint beneath appressed scales, separated by  
645 4-5× their diameter; intervals elevated.

646 **Abdominal sterna** Ventricle III anteromesally incurved around a fovea located mesally on anterior  
647 margin, posterior margin elevated and set off from IV along lateral 3/8s of its length. Sternum VII mesally  
648 2/3× as long as wide; setae slightly lengthening, and becoming medially directed in posterior 1/3; anterior  
649 margin weakly curved; posterior margin distinctly incurved mesally, appearing broadly notched; surface  
650 of sternite concave, appearing broadly foveate, immediately anteriad of marginal incurvature.

651 **Tergum** Tergum VII mesally incurved. Pygidium sub-cylindrical; medial 1/3 of anterior 2/3 of pygidium  
652 less sclerotized, with a patch of very short, fine setae.

653 **Sternum VIII** Anterior laminar edges each incurved forming a 130° angle with lateral margin; slightly  
654 less sclerotized medially between arms; posterior margin medially incurved.

655 **Ovipositor** Coxites as long as broad; styli with 3 setae near the base.

656 **Spermatheca** ?-shaped; collum short, apically with a large, angulate, hood-shaped projection angled  
657 at 45° to corpus, sub-equal in length to ramus and contiously aligned with curvature of bulb of ramus;  
658 collum sub-contiguous with, and angled at ca. 60° to ramus; ramus basally elongate and constricted,  
659 forming a stalk, 1/3× length of collum, bulbous apically, 3× thicker than stalk; corpus not swollen, of  
660 equal thickness to collum and cornu; cornu elongate, apically, gradually narrowed, strongly recurved in  
661 basal 1/3, straight along mesal 1/3, and curved near apical 1/3 such that apex is parallel to collum and  
662 corpus.

663 **Description of male**

664 Not available or known.

665 **Etymology**

666 Named in reference to the short, apically explanate setae interspersed throughout the dorsum, which give  
667 this species a distinctly “knobbed” appearance; *tylotos* – knobby; Greek adjective (Brown 1956).

668 **Material examined**

669 **Holotype** ♀ “H. O. Canyon.; Davis Mts., Texas; Jeff Davis County; VII-20-1968, 6200’; J. E. Hafernix”  
670 (**TAMU**).

671 **Paratypes** “24 mi. wsw. Ft. Davis; Jeff Davis Co., Texas; August 17, 1969; Board & Hafernix” (**TAMU**:  
672 1 ♀); “USA Texas Jeff Davis Co.; 4.1 mi. S. Fort Davis; sweeping grasses-weeds; 4750’ . 19.VII.82; R.S.  
673 Anderson” (**CMNC**: 1 ♀)

674 **Distribution**

675 This species has been found in three localities near the Davis Mountains in Jeff Davis County and in  
676 nearby Presidio County, Texas (USA). Habitat models (Figs. 5) predict that this represents the northeastern  
677 extent of its range, indicating a strong likelihood that it is present in other parts of the northern Chihuahuan  
678 desert, especially in the state of Chihuahua (México).

679 **Natural history**

680 No host plant associations have been documented. It is unknown whether this species is parthenogenetic.

681 **CHECKLIST OF SPECIES**

682 RCC-5 articulations are provided in **bold font**. See Jansen & Franz (2015) for alignments of *Minyomerus*  
683 concepts published from 1831 to 2015.

- Minyomerus* Horn, 1876: 17 sec. Jansen & Franz (2018)  
== (INT) AND > (**OST**) *Minyomerus* Horn, 1876 sec. Jansen & Franz (2015)  
> AND = *Elissa* Casey, 1888: 271 sec. Casey (1888)  
(synonymized by Kissinger, 1964: 30)  
> AND = *Pseudelissa* Casey, 1888: 273 sec. Casey (1888)  
(synonymized by Pierce, 1909: 359)  
> AND = *Piscatopus* Sleeper, 1960: 84 sec. Sleeper (1960)  
(synonymized by Jansen & Franz, 2015: 12)  
*microps* (Say, 1831: 9) sec. Jansen & Franz (2015) [redescribed, p. 45]  
== (INT) AND > (**OST**) AND = *Minyomerus innocuus* Horn, 1876: 18 sec. Horn (1876)  
[former type of *Minyomerus*, designated by Pierce, 1913: 400]  
(synonymized by Jansen & Franz, 2015: 45)  
== (INT) AND > (**OST**) AND = *Thylacites microps* Say, 1831: 9 sec. Say (1831)  
(transferred to *Minyomerus* on the authority of Buchanan *in litt.*  
by Blackwelder and Blackwelder, 1948: 46)  
== (INT) AND > (**OST**) AND = *Thylacites microsus* Boheman, 1833: 523 sec. Boheman (1833)  
(synonymized by LeConte, 1859: 286)  
*aeriballux* Jansen & Franz, 2015: 52 sec. Jansen & Franz (2015)  
*ampullaceus* sp. nov. sec. Jansen & Franz (2018)  
*bulbifrons* Jansen & Franz, 2015: 81 sec. Jansen & Franz (2015)  
*caseyi* (Sharp, 1891: 151) sec. Jansen & Franz (2015) [redescribed, p. 66]  
== AND = *Pseudelissa caseyi* Sharp, 1891: 151 sec. Sharp (1891)  
(generic name synonymized by Pierce, 1909: 359)  
*conicollis* Green, 1920: 194 sec. Jansen & Franz (2015) [redescribed, p. 33]  
*constrictus* (Casey, 1888: 272) sec. Jansen & Franz (2015) [redescribed, p. 22]  
== AND = *Elissa constricta* Casey, 1888: 272 sec. Casey (1888)  
(generic name synonymized by Kissinger, 1964: 30)  
*cracens* Jansen & Franz, 2015: 61 sec. Jansen & Franz (2015)  
*franko* sp. nov. sec. Jansen & Franz (2018)  
*gravivultus* Jansen & Franz, 2015: 92 sec. Jansen & Franz (2015)  
*griseus* (Sleeper, 1960: 84) sec. Jansen & Franz (2015) [redescribed, p. 96]  
== AND = *Piscatopus griseus* Sleeper, 1960: 84 sec. Sleeper (1960)  
(generic name synonymized by Jansen & Franz, 2015: 96)  
*imberbus* Jansen & Franz, 2015: 18 sec. Jansen & Franz (2015)  
*languidus* Horn, 1876: 18 sec. Jansen & Franz (2015) [redescribed, p. 40]  
== (INT) AND > (**OST**) *Minyomerus languidus* Horn, 1876: 18 sec. Horn (1876)  
== AND = *Pseudelissa cinerea* Casey, 1888: 274 sec. Casey (1888)  
(synonymized by Pierce, 1909: 359)  
*laticeps* (Casey, 1888: 272) sec. Jansen & Franz (2015) [redescribed, p. 27]  
== AND = *Elissa laticeps* Casey, 1888: 272 sec. Casey (1888)  
(generic name synonymized by Kissinger, 1964: 30)  
*politus* Jansen & Franz, 2015: 86 sec. Jansen & Franz (2015)  
*puticulatus* Jansen & Franz, 2015: 75 sec. Jansen & Franz (2015)  
*reburrus* Jansen & Franz, 2015: 57 sec. Jansen & Franz (2015)  
*rutellirostris* Jansen & Franz, 2015: 103 sec. Jansen & Franz (2015)  
*sculptilis* sp. nov. sec. Jansen & Franz (2018)  
*trisetosus* Jansen & Franz, 2015: 71 sec. Jansen & Franz (2015)  
*tylotos* sp. nov. sec. Jansen & Franz (2018)

684 **SPECIES IDENTIFICATION KEY**

- 1 Procoxae apparently separate, with intercoxal processes touching or very nearly so ..... 2
- Procoxae apparently contiguous, with intercoxal processes short and not touching ..... 3
- 2 (1) Rostrum approximately square and as wide as head in dorsal view; ramus of spermatheca basally narrow, forming a stalk that tapers into an apical bulb.....  
..... *Minyomerus rutellirostris* [JF2015]
- Rostrum approximately trapezoidal and narrower than the head in dorsal view; ramus of spermatheca cylindrical, somewhat bulbous, and basally constricted ..  
..... *Minyomerus griseus* [JF2015]
- 3 (1) Anterior margin of pronotum bearing a full, well-developed tuft of 10 or more ocular vibrissae; anterolateral margins of prementum explanate, angular, and posteriorly declivous, with a distinctly hexagonal appearance..... 4
- Ocular vibrissae reduced in number or length; anterior margins of prementum not explanate and declivous, typically with a pentagonal appearance ..... 5
- 4 (3) Head very wide and only somewhat swollen between eyes; rostrum ca. 4× wider than long in dorsal view; pronotum in dorsal view cylindrical; elytral setae short, brown, and sub-recumbent; ramus of spermatheca stalked and with apical bulb abruptly constricted, not tapering at point of connection to stalk ..... *Minyomerus laticeps* [JF2015]
- Head and rostrum typical (rostrum 2-3× wider than long in dorsal view); pronotum in dorsal view somewhat globular, with a strong anterior constriction; elytral setae short and setiform, especially near disk; spermatheca without basal stalk ..  
..... *Minyomerus constrictus* [JF2015]
- 5 (3) Metatibial apex strongly convex, with setae similar in length to those of remainder of leg, somewhat lighter in color and translucent, and slightly lamelliform; head somewhat conical in form, rounded between the eyes; elytral setae copious, not in uniform rows on intervals, instead appearing in offset rows, especially near elytral suture and declivity ..... 6
- Metatibial apex oblique or weakly convex, with setae short and conical in appearance; head roughly quadrate; elytral setae in relatively uniform rows on elytra, not strongly offset.... 7
- 6 (5) Elytral striae deeply and distinctly punctate, appearing pin-striped; elytra without obvious humeri, gradually widening posteriorly; ramus of spermatheca elongate, annulate, and sub-apically situated on corpus..... *Minyomerus aeriballux* [JF2015]
- Elytral striae punctate, with punctures somewhat obscured by appressed scales; elytra somewhat pyriform, with weak, but obviously present humeri; ramus of spermatheca elongate, somewhat swollen, and sub-apically situated on corpus ..  
..... *Minyomerus reburrus* [JF2015]
- 7 (5) Elytra very strongly convex in lateral view; anterior margin of pronotum wider than posterior margin; spermatheca comma-shaped, with ramus reduced, apically flattened and sub-contiguous with the collum; aedeagal pedon membranous ventrally, and not fully sclerotized ..  
..... *Minyomerus conicollis* [JF2015]
- Elytra only somewhat convex to nearly flat in lateral view; anterior margin of pronotum similar in length to posterior margin; spermatheca variable; aedeagal pedon fully sclerotized ..  
..... 8
- 8 (7) Body shape distinctly flask-like, with strongly constricted, sub-cylindrical pronotum and greatly protuberant elytra; in dorsal view, elytra nearly 2× width of pronotum at maximum width and nearly 3/4× as wide as long; in lateral view, anterior and posterior declivities of elytra abrupt and nearly vertical, with anterior elytral margin projecting strongly and characteristically dorsad of articulation with posterior pronotal margin; corpus of spermatheca with highly elongate projection aligned with midline of the ramus, which is basally tapered and angled at nearly 45° to corpus .. *Minyomerus ampullaceus* [JF2018], sp. n.

- Body shape usually narrow; elytra typically not more than  $1.5 \times$  width of pronotum and typically not more than  $2/3 \times$  as wide as long in dorsal view; elytral declivities in lateral view variable, but anterior margin never abruptly and strongly projected dorsad of posterior pronotal margin; spermatheca variable, but never with elongate projection aligned with midline of ramus ..... 9
- 9 (8) Setae of elytral disc a mix of shorter, brown setae and longer, more erect, white setae ..... 10
- Setae of elytral disc uniform ..... 12
- 10 (9) Anterior margin of pronotum bearing strikingly long setae, which project laterally up to  $80^\circ$  from longitudinal body axis and at least equal to diameter of eye; spermatheca with short, somewhat bulbous corpus, ramus sub-equal in size and perpendicular to corpus, and collum strongly recurved along basal  $1/3$  of its length; aedeagal pedon relatively short and wide, and abruptly constricted in apical  $1/5$ , thereafter tapered to rounded point ..... *Minyomerus franko* [JF2018], sp. n.
- Anterior margin of pronotum bearing setae more strongly directed anteriorly and never as long as diameter of eye; spermatheca variable; aedeagal pedon, where known, narrow and expanded laterally in region of ostium ..... 11
- 11 (10) Setae apically explanate, appearing somewhat spatulate; corpus of spermatheca uniquely elongate, ramus short and cylindrical ..... *Minyomerus caseyi* [JF2015]
- Setae linear; corpus of spermatheca typical, ramus bulbous and basally constricted ..... *Minyomerus trisetosus* [JF2015]
- 12 (9) Anterior margin of pronotum lined with linear setae that extend anteriorly beyond margin by half their length ..... 13
- 686 – Anterior margin of pronotum lacking setae, or with setae that do not extend far beyond margin ..... 14
- 13 (12) Lateral margins of gular cavity strongly rounded, never straight, and slightly longer than posterior margin; frons weakly projected between eyes; appressed scales on elytra without opalescent sheen; nasal plate with or without metallic reflections; lamina of spiculum ventrale sclerotized throughout ..... *Minyomerus languidus* [JF2015]
- Lateral margins of gular cavity nearly straight, and not longer than posterior margin; frons strongly projected between eyes; appressed scales with strong opalescent sheen; nasal plate with metallic reflections; lamina of spiculum ventrale with a membranous region present medially between laminar arm ..... *Minyomerus gravivultus* [JF2015]
- 14 (12) Elytra each  $4-5 \times$  as long as broad in dorsal view, strongly punctate; elytra constricted anteriad of humeri, narrower than the pronotum, widening thereafter near the humeri; spermatheca with the corpus somewhat bulbous, and the ramus either flattened somewhat or slightly elongate ..... *Minyomerus cracens* [JF2015]
- Elytra not so elongate, variably punctate; elytra lacking basal constriction; spermatheca variable ..... 15
- 15 (14) Elytral striae with large, obvious punctures ..... 16
- Elytral striae without evident punctures ..... 17
- 16 (15) Frons strongly protuberant; elytra in lateral view convex dorsally; spermatheca with corpus possessing an annulate, rectate projection nearly  $1/2 \times$  length of ramus; aedeagal pedon evenly curving towards apex; aedeagal flagellum with spiriform apical sclerite that spirals counterclockwise and of equal length to aedeagal pedon ..... *Minyomerus bulbifrons* [JF2015]

- Frons not so protuberant; elytra in lateral view nearly flat dorsally; spermatheca with corpus possessing an annulate, rectate projection nearly  $2/3 \times$  length of the ramus; aedeagal pedon narrow and elongate; aedeagal flagellum with very minute apical sclerite ..... *Minyomerus puticulatus* [JF2015]
- 17 (15) Frons strongly protruding in lateral view by ca.  $2 \times$  diameter of eye ..... 18
- Frons not or weakly protruding in lateral view by  $1.5 \times$  diameter of eye or less ..... 19
- 18 (17) Nasal plate defined by inversely V-shaped, impressed lines; spermatheca with the ramus elongate and apically swollen, corpus possessing an annulate, rectate projection nearly  $1/2 \times$  length of the ramus, and cornu evenly recurved throughout its length; aedeagal flagellum with a spiriform apical sclerite that spirals clockwise and of equal length to pedon ..... *Minyomerus politus* [JF2015]
- Nasal plate lacking distinct impressions; spermatheca with ramus basally tapered with a short stalk, corpus narrow and lacking an annulate rectate bulb, and cornu with an abrupt apical curve; males not known ..... *Minyomerus tylotos* [JF2018], sp. n.
- 19 (17) Ventrolateral sulci weakly defined as a notch ventrad of antennal insertion, or absent entirely; intervals broadly sculpted and raised, and striae not punctate; body generally robust in overall quality; appressed scales uniformly beige and gray, with a distinctly ‘crusty’ appearance; spermatheca with ramus and collum appearing as two subcontiguous, apically invaginated bulbs ..... *Minyomerus microps* [JF2015]
- Ventrolateral sulci deeply and distinctly defined along their entire length; intervals, if raised, only sculpted along lateral faces of elytra, not on disk; body usually not markedly robust; appressed scales either translucent or otherwise typical of genus, not beige and crusted; spermatheca distinctly sinuate, with well defined, protruding ramus ..... 20
- 20 (19) Elytra with very minute setae, only perceptible at high magnification; lateral faces of elytra with intervals not noticeably raised; ramus of spermatheca elongate, cylindrical, and slightly thinner than corpus, cornu strongly recurved in basal half with uniquely sinuate appearance, both corpus and cornu with hood-like projections shorter than ramus; males not known ..... *Minyomerus imberbus* [JF2015]
- Elytra with easily visible, linear setae; lateral faces of elytra with intervals raised; ramus of spermatheca bulbous, basally tapered, and similar in width to corpus, cornu strongly recurved, but short in basal half with uniquely sinuate appearance, both corpus and cornu with hood-like projections longer than ramus; aedeagal pedon narrow and cylindrical, apically tapered .... *Minyomerus sculptilis* [JF2018], sp. n.

## 688 PHYLOGENETIC RESULTS

689 A matrix of 52 characters was assembled for the 26 terminal taxa (Tab. 1). These characters are comprised  
 690 of all 46 characters included in the revision of *Minyomerus* [JF2015], plus an additional 6 characters  
 691 intended to identify putative sister taxa to the newly described species. Parsimony analysis returned a  
 692 single, most-parsimonious cladogram (henceforth MPT) with a length (L) of 99 steps, a consistency index  
 693 (CI) of 60 and a retention index (RI) of 80 (Farris 1989); see Figs. 37-38. TNT (Tree Analysis Using  
 694 New Technology) was used to confirm that the shortest tree had been found (Goloboff et al. 2008). The  
 695 most-parsimonious cladogram is shown in Fig. 37, with relative and absolute Bremer support values  
 696 (see also **Materials and Methods: Phylogenetic analysis**) mapped along the left side of each branch;  
 697 nodes with bootstrap support above 0.95 are marked with a “\*” symbol to the right of each node. In a  
 698 complementary graph, we show the herein used clade concept labels (Fig. 38).

699 The characters, states, and preferred optimizations are described in this section. Characters relating  
 700 to placement of the herein described taxa are discussed in detail in the **Discussion** section, along with  
 701 changes in species group composition and tree topology from Jansen & Franz (2015). For all characters  
 702 not resolved as unreversed synapomorphies, both the individual consistency (ci) and retention (ri) indices  
 703 are provided.

**Table 1. Taxon/character matrix used for for cladistic analysis.** Includes all species of *Minyomerus* [JF2015], newly designated species, and select outgroup taxa. All multi-state characters coded as additive, except for character 33. The symbol “–” denotes inapplicable character states, whereas “?” denotes missing information (see also text).

Taxon \ Character	0	1	1	2	2	3	3	4	4	5
	5	0	5	0	5	0	5	0	5	0
<i>Sitona californicus</i> [non-focal]	00-00	?????	00000	00000	00000	00000	00---	-0---	--???	????? ??
<i>Pandeleteius cinereus</i> [non-focal]	11000	?????	01000	00001	01000	00100	00000	000-0	00???	????? ??
<i>Pandeleteinus subcancer</i> [non-focal]	11000	?????	01000	00001	01010	00100	00000	000-0	00???	????? ??
<i>Isodrusus debilis</i> [non-focal]	11000	?????	01000	00001	01011	00100	00000	000-0	00???	????? ??
<i>Isodacrys buchanani</i> [non-focal]	11000	?????	01000	00001	01011	00100	00000	000-0	00???	????? ??
<i>Minyomerus constrictus</i> [JF2015]	21100	00010	02110	01002	00011	11211	00000	00000	01010	00
<i>Minyomerus laticeps</i> [JF2015]	21100	00010	02110	01002	00011	11211	00000	00000	01010	00
<i>Minyomerus imberbus</i> [JF2015]	21100	?????	02010	11002	10011	11211	01001	00000	00???	????? ??
<i>Minyomerus scutipilis</i> [JF2018]	21100	?????	02010	11002	10011	11211	01001	00000	00001	00000 10
<i>Minyomerus conicollis</i> [JF2015]	21100	00000	02010	11002	10011	10211	00001	10000	01000	00000 00
<i>Minyomerus languidus</i> [JF2015]	21000	11100	02010	11002	10011	10211	00001	10000	?????	????? ??
<i>Minyomerus microps</i> [JF2015]	21001	11101	02110	11002	10011	10211	00001	10000	10???	????? ??
<i>Minyomerus tytulos</i> [JF2018]	21001	11101	02110	11002	10011	10211	00001	10000	00???	????? ??
<i>Minyomerus cracens</i> [JF2015]	21000	11101	02020	11112	10011	11211	00001	10001	00000	10010 10
<i>Minyomerus ampullaceus</i> [JF2018]	21000	?????	02020	11???	10011	11211	00001	11001	00???	????? ??
<i>Minyomerus aeriballus</i> [JF2015]	22000	11101	12020	11012	10011	20211	00001	11001	10000	00000 01
<i>Minyomerus reburrus</i> [JF2015]	22000	11101	12020	11112	10011	20211	00001	11021	00???	????? ??
<i>Minyomerus franko</i> [JF2018]	21110	10100	02020	11002	10011	11211	00001	10011	10010	00000 01
<i>Minyomerus caseyi</i> [JF2015]	21110	00101	02020	11112	10011	11211	00001	10101	10010	10010 01
<i>Minyomerus trisetosus</i> [JF2015]	21110	00101	02020	11012	10011	10211	00001	10101	10???	????? ??
<i>Minyomerus gravivultus</i> [JF2015]	21100	11101	02120	11002	10011	10211	00111	10000	??010	00000 11
<i>Minyomerus griseus</i> [JF2015]	21100	10101	02120	01002	10111	11211	00111	10000	00010	01100 10
<i>Minyomerus rutellirostris</i> [JF2015]	21100	10101	02120	11002	10111	11211	00111	10000	00010	01100 10
<i>Minyomerus puticulatus</i> [JF2015]	21000	11101	02020	11012	10011	11211	10101	10010	01011	01000 11
<i>Minyomerus bulbifrons</i> [JF2015]	21000	11101	02021	11112	10011	10211	10101	10000	01110	01001 01
<i>Minyomerus politus</i> [JF2015]	21000	?????	02021	11112	10011	10211	10101	10010	01111	01001 11

- 704 1. Habitus, form of appressed scales: (0) elongate pyriform, not overlapping; (1) sub-circular to  
 705 polygonal, variously overlapping non-linearly; (2) sub-circular and only overlapping posteriorly.  
 706 Coded as additive due to alignment of character states with the preferred phylogeny. Coding as  
 707 non-additive in isolation or in unison with other additive multi-state characters does not affect  
 708 polarization of the character/states or alter the phylogeny. State 1 is a synapomorphy for the  
 709 tanytmecine clade [non-focal], whereas state 2 is a synapomorphy for *Minyomerus* [JF2018].
- 710 2. Habitus, arrangement of elytral setae: (0) variously interspersed; (1) arranged in single-file rows  
 711 on elytral intervals; (2) arranged non-uniformly on elytral intervals. Coded as additive due to  
 712 alignment of character states with the preferred phylogeny. Coding as non-additive in isolation or in  
 713 unison with other additive multi-state characters does not affect polarization of the character/states

714 or alter the phylogeny. State 1 is a synapomorphy for the tanytarsine clade [non-focal], whereas  
715 state 2 is a synapomorphy for the *M. aeriballus*–*M. reburrus* clade [JF2015].

- 716 3. Habitus, lateral elytral setae and ventral setae differentiated from setae of elytral disc: (0) absent;  
717 (1) present. Homoplasy for *Minyomerus* [JF2018], with a reversal (state 0) in the *M. aeriballus*–*M.*  
718 *languidus* clade [JF2015], subsequent convergent gain (state 1) in the *M. bulbifrons*–*M. caseyi* clade  
719 [JF2018], and convergent reversal (state 0) in the *M. bulbifrons*–*M. puticalutus* clade [JF2015] (ci =  
720 25; ri = 70).
- 721 4. Habitus, rows of elytral setae with larger white setae randomly interspersed among smaller brown  
722 setae: (0) absent; (1) present. Synapomorphy for the *M. caseyi*–*M. franko* clade [JF2018]. Changed  
723 from Jansen & Franz (2015), where *M. rutellirostris* [JF2015] was previously coded as having this  
724 character; however, the white elytral setae of this species are not randomly interspersed, but follow  
725 a distinct, and uniquely derived, pattern where every other interval contains a row of such setae.
- 726 5. Habitus, elytra and pronotum generally large, protuberant, and sculpted in appearance along dorsal  
727 and lateral faces: (0) absent; (1) present. Synapomorphy for the *M. microps*–*M. tylotos* clade  
728 [JF2018].
- 729 6. Prementum, anterior margin medially with a distinct facet, rather than a single edge edge, that  
730 continues to lateral margins: (0) absent; (1) present. Synapomorphy for the *M. aeriballus*–*M.*  
731 *languidus* clade [JF2015], with a single reversal in the *M. caseyi*–*M. trisetosus* clade [JF2015] (ci =  
732 50; ri = 75).
- 733 7. Prementum, strongly ligulate and with margins nearly straight, appearing pentagonal: (0) absent;  
734 (1) present. Synapomorphy for the *M. aeriballus*–*M. languidus* clade [JF2015], with independent  
735 reversals in the *M. caseyi*–*M. franko* clade [JF2018] and *M. griseus*–*M. rutellirostris* clade [JF2015],  
736 respectively (ci = 33; ri = 71).
- 737 8. Prementum, anterolateral margins simple, unexpanded: (0) absent; (1) present. Synapomorphy for  
738 the *M. aeriballus*–*M. languidus* clade [JF2015].
- 739 9. Prementum, anterolateral margins explanate, angular, and posteriorly declivous, with a distinctly  
740 hexagonal appearance: (0) absent; (1) present. ACCTRAN optimization preferred (see Agnarsson  
741 & Miller 2008), therefore inferred as a synapomorphy for the *M. constrictus*–*M. laticeps* clade  
742 [JF2015].
- 743 10. Prementum, exposure of palpomere I: (0) exposed, visible beyond ligula and anterior margin of  
744 prementum in ventral view; (1) hidden, fully covered or only minutely exposed beyond ligula and  
745 anterior margin of prementum in ventral view. Synapomorphy for the *M. aeriballus*–*M. microps*  
746 clade [JF2015], with a single reversal in *M. franko* [JF2018] (ci = 50; ri = 75).
- 747 11. Rostrum, form in dorsal view: (0) approximately quadrate; (1) somewhat conical, medially convex.  
748 Synapomorphy for the *M. aeriballus*–*M. reburrus* clade [JF2015].
- 749 12. Rostrum, form of nasal plate and demarcation of epistoma: (0) with three parallel, longitudinal cari-  
750 nae, and surface planar between these; (1) with a sharp, narrow, chevron-shaped carina demarcating  
751 epistoma; (2) with a broad, scale-covered, chevron-shaped carina demarcating epistoma. Coded  
752 as additive due to alignment of character states with preferred phylogeny. Coding as non-additive  
753 in isolation or in unison with other additive multi-state characters does not affect polarization of  
754 the character/states or alter the phylogeny. State 1 is a synapomorphy for the tanytarsine clade  
755 [non-focal], whereas state 2 is a synapomorphy for *Minyomerus* [JF2018].
- 756 13. Rostrum, sulcus posteriad of nasal plate weakly impressed: (0) absent; (1) present. Convergently  
757 present in the *M. constrictus*–*M. laticeps* clade [JF2015], the *M. microps*–*M. tylotos* clade [JF2018],  
758 and the *M. gravivultus*–*M. griseus* clade [JF2015] (ci = 33; ri = 60).
- 759 14. Rostrum, form of sulcus posteriad of nasal plate: (0) absent; (1) sulcus present, broad, and weakly  
760 punctate; (2) sulcus present, more strongly punctate. Coded as additive due to alignment of character  
761 states with preferred phylogeny. Coding as non-additive in isolation or in unison with other additive

762 multi-state characters does not affect polarization of the character/states or alter the phylogeny.  
763 Synapomorphy for *Minyomerus* [JF2018] (state 1) and the *M. aeriballux*–*M. cracens* clade [JF2015]  
764 (state 2), respectively.

- 765 15. Head, frons very strongly projected beyond anterior margin of eye, by 2× anterior-posterior length  
766 of eye: (0) absent; (1) present. Synapomorphy for the *M. bulbifrons*–*M. politus* clade [JF2015].
- 767 16. Head, frons with posterior transverse constriction: (0) absent; (1) present. Synapomorphy for the *M.*  
768 *aeriballux*–*M. languidus* clade [JF2015], with a single reversal in *M. griseus* [JF2015] (ci = 50, ri =  
769 85).
- 770 17. Antenna, length of scrobe relative to funicle and club: (0) scrobe shorter than funicle and club com-  
771 bined; (1) scrobe subequal in length to funicle and club combined. Synapomorphy for *Minyomerus*  
772 [JF2018].
- 773 18. Antenna, terminal funicular segment entirely without thin, nearly setiform scales: (0) absent; (1)  
774 present. Convergently present in *M. cracens* [JF2015], *M. reburrus* [JF2015], *M. caseyi* [JF2015],  
775 and the *M. bulbifrons*–*M. politus* clade [JF2015] (ci = 25; ri = 25).
- 776 19. Antenna, terminal funicular segment at least partially clothed with broad scales: (0) absent; (1)  
777 present. Synapomorphy for the *M. aeriballux*–*M. cracens* clade [JF2018] with independent reversals  
778 in *M. franko* [JF2018] and the *M. gravivultus*–*M. griseus* clade [JF2015] (ci = 33; ri = 71).
- 779 20. Head, angle of base in relation to prothorax: (0) directed anteriorly, in line with main body axis; (1)  
780 directed strongly ventrally; (2) directed slightly ventrally. Coded as additive due to alignment of  
781 character states with preferred phylogeny. Coding as non-additive in isolation or in unison with  
782 other additive multi-state characters does not affect polarization of the character/states or alter the  
783 phylogeny. State 1 is a synapomorphy for the tanymecine clade [non-focal], whereas state 2 is a  
784 synapomorphy for *Minyomerus* [JF2018].
- 785 21. Pronotum, condition of post-ocular vibrissae: (0) present in a well-developed tuft of 10 or more  
786 setae; (1) present in a reduced tuft of 3-7 setae. Synapomorphy for the *M. aeriballux*–*M. imberbus*  
787 clade [JF2018].
- 788 22. Prosternum, intercoxal process complete, undivided: (0) absent; (1) present. Synapomorphy for the  
789 tanymecine clade [non-focal], with a single reversal for *Minyomerus* [JF2018] (ci = 50; ri = 66).
- 790 23. Prosternum, intercoxal process divided at midpoint between coxae, but both anterior and posterior  
791 processes extending completely between procoxae and contiguous with each other: (0) absent; (1)  
792 present. Synapomorphy for the *M. griseus*–*M. rutellirostis* clade [JF2015].
- 793 24. Legs, fore femora not swollen in comparison to other legs: (0) absent; (1) present. Synapomorphy  
794 for the *M. aeriballux*–*P. subcancer* clade [non-focal].
- 795 25. Legs, sculpture of ventral surface of protibiae: (0) evenly convex throughout; (1) with a longitudinal  
796 groove or concavity. Synapomorphy for the *M. aeriballux*–*I. debilis* clade [non-focal].
- 797 26. Legs, setation of metatibial apex: (0) bristles at least as long as surrounding setae and setiform; (1)  
798 bristles shorter than surrounding setae and conical; (2) bristles sub-equal in length to surrounding  
799 setae and somewhat lamelliform. Coded as additive due to alignment of character states with  
800 preferred phylogeny, and the appearance of being a transformation series. Coding as non-additive  
801 in isolation or in unison with other additive multi-state characters does not affect polarization of the  
802 character/states or alter the phylogeny. Synapomorphy for *Minyomerus* [JF2018] (state 1) and the  
803 *M. aeriballux*–*M. reburrus* clade [JF2015] (state 2), respectively.
- 804 27. Legs, curvature of metatibial apex: (0) convex ; (1) oblique. ACCTRAN optimization preferred  
805 (see Agnarsson & Miller 2008), therefore inferred as a synapomorphy for *Minyomerus* [JF2018]  
806 with a reversal (state 0) in the *M. aeriballux*–*M. conicollis* clade [JF2015], then a convergent gain  
807 (state 1) in the *M. aeriballux*–*M. bulbifrons* clade [JF2018], with independent reversals (state 0) in  
808 the *M. aeriballux*–*M. reburrus* clade [JF2015], *M. gravivultus* [JF2015], *M. trisetosus* [JF2015],  
809 and the *M. bulbifrons*–*M. politus* clade [JF2015] (ci = 14; ri = 40).

- 810 28. Legs, relative length of mesotarsi to mesotibiae: (0) tarsi less than  $3/4 \times$  length of tibiae; (1)  
 811 tarsi at least equal in length to tibiae; (2) tarsi shorter than tibiae, but longer than  $3/4 \times$  length of  
 812 tibiae. Coded as additive due to alignment of character states with preferred phylogeny. Coding  
 813 as non-additive in isolation or in unison with other additive multi-state characters does not affect  
 814 polarization of the character/states or alter the phylogeny. State 1 is a synapomorphy for the  
 815 tanymecine clade [non-focal], whereas state 2 is a synapomorphy for *Minyomerus* [JF2018].
- 816 29. Legs, tarsi ventrally spinose: (0) absent; (1) present. Synapomorphy for *Minyomerus* [JF2018].
- 817 30. Elytra, humeral angle rounded, not projected: (0) absent; (1) present. Synapomorphy for the *M.*  
 818 *aeriballux*–*I. buchanani* clade [non-focal].
- 819 31. Female terminalia, spermatheca with apical cylindrical bulb on corpus: (0) absent; (1) present.  
 820 Synapomorphy for the *M. bulbifrons*–*M. puticulatus* clade [JF2015].
- 821 32. Female terminalia, corpus of spermatheca sinuate: (0) absent; (1) present. Synapomorphy for the  
 822 *M. imberbus*–*M. sculptilis* clade [JF2018].
- 823 33. Female terminalia, lamina of spiculum ventrale less sclerotized between laminar arms: (0) absent;  
 824 (1) present. Coded as inapplicable for *S. californicus* [non-focal], as laminar arms are not apparent.  
 825 Synapomorphy for the *M. gravivultus*–*M. griseus* clade [JF2015].
- 826 34. Female terminalia, lamina of spiculum ventrale with laminar arms bifurcating around a membranous  
 827 region: (0) absent; (1) present. Coded as inapplicable for *S. californicus* [non-focal], as laminar  
 828 arms are not apparent. Synapomorphy for the *M. gravivultus*–*M. griseus* clade [JF2015].
- 829 35. Female terminalia, lamina of spiculum ventrale with style basally divided or obscured, not mesally  
 830 intact: (0) absent; (1) present. Coded as inapplicable for *S. californicus* [non-focal], as laminar  
 831 arms are not apparent. Synapomorphy for the *M. aeriballux*–*M. imberbus* clade [JF2015].
- 832 36. Female terminalia, lamina of spiculum ventrale with laminar arms clearly bifurcating. (0) absent;  
 833 (1) present. Coded as inapplicable for *S. californicus* [non-focal], as laminar arms are not apparent.  
 834 Synapomorphy for the *M. aeriballux*–*M. conicollis* clade [JF2015].
- 835 37. Female terminalia, laminar arms narrowly bifurcating basally, thereafter sub-parallel mesally: (0)  
 836 absent; (1) present. Synapomorphy for the *M. aeriballux*–*M. ampullaceus* clade [JF2018].
- 837 38. Female terminalia, coxites of ovipositor with a lateral, anteriorly-directed, recurved, alate process:  
 838 (0) absent; (1) present. Coded as inapplicable for *S. californicus* [non-focal], as coxites of ovipositor  
 839 are not apparent. Synapomorphy for the *M. caseyi*–*M. trisetosus* clade [JF2015].
- 840 39. Female terminalia, relative length of styli to coxites of ovipositor: (0) Similar in size; (1) distinctly  
 841 shortened; (2) highly reduced, appearing minute. Coded as non-additive, due to strong differences  
 842 in structure of coxites and styli in state 2; inapplicable for outgroup taxa, as styli of ovipositor are  
 843 not apparent. ACCTRAN optimization preferred (see Agnarsson & Miller 2008), therefore inferred  
 844 as convergent gains in *M. franko* [JF2018] and the *M. bulbifrons*–*M. puticulatus* clade [JF2015]  
 845 (state 1), with a single reversal in *M. bulbifrons* [JF2015] (state 0). Autapomorphy for *M. reburrus*  
 846 [JF2015] (state 2) (ci = 50, ri = 0).
- 847 40. Female terminalia, condition of medial, anteriorly-directed, sclerotized process of coxites of  
 848 ovipositor: (0) fully developed; (1) reduced and inapparent. Coded as inapplicable for *S. californicus*  
 849 [non-focal], as coxites of ovipositor are not apparent. Synapomorphy for the *M. aeriballux*–*M.*  
 850 *cracens* clade [JF2015], with a single reversal in the *M. gravivultus*–*M. griseus* clade [JF2015] (ci  
 851 = 50, ri = 83).
- 852 41. Female terminalia, anterior margin of tergum VII entirely free of sclerotized band: (0) absent;  
 853 (1) present. Coded as inapplicable for *S. californicus* [non-focal], as the tergum VII is evenly  
 854 sclerotized throughout. Convergently present in *M. aeriballux* [JF2015], *M. microps* [JF2015], and  
 855 the *M. caseyi*–*M. trisetosus* clade [JF2018] (ci = 33; ri = 50).

- 856 42. Female terminalia, anterior margin of tergum VII sclerotized fully, appearing as an obviously  
 857 complete band: (0) absent; (1) present. Coded as inapplicable for *S. californicus* [non-focal], as the  
 858 tergum VII is evenly sclerotized throughout. Convergently present in *M. conicollis* [JF2015] and  
 859 the *M. bulbifrons*–*M. puticulatus* clade [JF2015] (ci = 50; ri = 66).
- 860 43. Male terminalia, apical sclerite of aedeagal flagellum elongate-spiriform: (0) absent; (1) present.  
 861 Synapomorphy for the *M. bulbifrons*–*M. politus* clade [JF2015].
- 862 44. Male terminalia, style of spiculum gastrale with an anterior ventral flange: (0) absent; (1) present.  
 863 Synapomorphy for the *M. bulbifrons*–*M. caseyi* clade [JF2018].
- 864 45. Male terminalia, lamina of spiculum gastrale longer than broad and anteriorly extended along  
 865 syle: (0) absent; (1) present. ACCTRAN optimization preferred (see Agnarsson & Miller 2008),  
 866 therefore inferred as convergent gains in the *M. imberbus*–*M. sculptilis* clade [JF2018] and the *M.*  
 867 *bulbifrons*–*M. puticulatus* clade [JF2015], with a reversal in *M. bulbifrons* [JF2015] (ci = 33; ri =  
 868 0).
- 869 46. Male terminalia, sub-triangular sclerites of sternum VIII with a medial process: (0) absent; (1)  
 870 present. ACCTRAN optimization preferred (see Agnarsson & Miller 2008), therefore inferred as  
 871 convergent gains in *M. cracens* [JF2015] and the *M. caseyi*–*M. trisetosus* clade [JF2015] (ci =  
 872 50, ri = 0).
- 873 47. Male terminalia, curvature of posterior margin of tergum VII: (0) evenly arcuate; (1) medially  
 874 incurved. ACCTRAN optimization preferred (see Agnarsson & Miller 2008), therefore convergently  
 875 present in the *M. constrictus*–*M. laticeps* clade [JF2015] and the *M. bulbifrons*–*M. gravivultus* clade  
 876 [JF2015] with a reversal in *M. gravivultus* [JF2015] (ci = 33; ri = 66).
- 877 48. Male terminalia, tergum VII approximately 4× as long as broad: (0) absent; (1) present. Synapo-  
 878 mory for the *M. griseus*–*M. rutellirostris* clade [JF2015].
- 879 49. Male terminalia, aedeagal pedon expanded laterally around ostium: (0) absent; (1) present. ACC-  
 880 TRAN optimization preferred (see Agnarsson & Miller 2008), therefore convergently present in the  
 881 *M. constrictus*–*M. laticeps* clade [JF2015], *M. cracens* [JF2015], and the *M. caseyi*–*M. trisetosus*  
 882 clade [JF2015] (ci = 33; ri = 33).
- 883 50. Male terminalia, aedeagal pedon broad basally, evenly tapering toward apex: (0) absent; (1) present.  
 884 Synapomorphy for the *M. bulbifrons*–*M. politus* clade [JF2015].
- 885 51. Male terminalia, aedeagal pedon medially sclerotized along dorsum: (0) absent; (1) present.  
 886 ACCTRAN optimization preferred (see Agnarsson & Miller 2008), therefore convergently present  
 887 in the *M. imberbus*–*M. sculptilis* clade [JF2015], *M. cracens* [JF2015], and the *M. bulbifrons*–*M.*  
 888 *gravivultus* clade [JF2015], with a reversal in *M. bulbifrons* [JF2015] (ci = 25; ri = 50).
- 889 52. Male terminalia, width of connection between apodemes of aedeagal tegmen: (0) wider than base of  
 890 apodeme; (1) narrower than base of apodeme. Synapomorphy for the *M. aeriballux*–*M. bulbifrons*  
 891 clade [JF2018], with a single reversal in the *M. griseus*–*M. rutellirostris* clade [JF2011] (ci = 50; ri  
 892 = 83).

## 893 RCC–5 ALIGNMENTS

894 Details of our RCC–5 alignment approached are given in free text form in the **Supplemental Information**  
 895 **SI1**, which also describes the content of the data input and output files. The latter, in turn, are appended  
 896 in .txt, .csv, and .pdf format in the **Supplemental Information SI2 to S4**. All shown alignments are  
 897 *intensional* in the sense of Franz & Peet (2009), and thus maximize high-level concept congruence where  
 898 indicated, and in spite of non-congruent lower-level concept sampling.

899 The first, classification-based alignment (Fig. 1) is simple and straightforward to interpret (see also  
 900 **Supplemental Information SI2**). We obtain high-level congruence among the concepts *Minyomerus*  
 901 [JF2018] and *Minyomerus* [JF2015], where 17 species-level concepts are retained from Jansen & Franz  
 902 (2015) and four species-level concepts are added in the current review. The coverage constraint is relaxed

for *Minyomerus* [JF2015], thus allowing the four new species-level concepts to be subsumed under this parent. This is based on our assertion that they fall under the generic character circumscription of Jansen & Franz (2015).

The following two Figs. 2-3 show fully bifurcated, multi-phylogeny alignments of the same reasoner toolkit input, but resolved as whole concepts versus split concepts, respectively. In Fig. 2 (**Supplemental Information SI3**), we observe that the phylogenetic placements of *two* of the four new species-level concepts cause significant non-congruence in the alignment, resulting in seven overlapping RCC-5 articulations. *Minyomerus franko* [JF2018] is subsumed under the *M. caseyi*-*M. franko* clade [JF2018], which is intensionally congruent with the *M. caseyi*-*M. trisetosus* clade [JF2015]. In other words, this placement is not the source of non-congruence in the alignment. Similarly, the placement of *M. tylotos* [JF2018] into the new *M. microps*-*M. tylotos* clade [JF2018] is not conflicting in an intensional sense. At the next, more inclusive level, this addition "resolves" into the congruent *M. aeriballux*-*M. microps* clade [JF2018]/[JF2015].

In contrast, the placement of *M. ampullaceus* [JF2018] "inside" of *M. cracens* [JF2015] in the current phylogeny, generates five overlapping articulations among as many (five) non-congruent concept regions positioned 1-2 levels above these species-level concepts. The conflict is resolved in the next, more inclusive and congruent region of the *M. aeriballux*-*M. cracens* clade [JF2018] == *M. aeriballux*-*M. bulbifrons* clade [JF2015]

The placements of the previously circumscribed *M. imberbus* [JF2015] and the new species-level concept *M. sculptilis* [JF2018] - in relation to the congruent clade *M. constrictus*-*M. laticeps* [JF2018]/[JF2015] - cause two additional instances of overlap (Fig. 2). In the current phylogeny, *M. imberbus* [JF2015] is sister to *M. sculptilis* [JF2018], and placed "inside" of the *M. constrictus*-*M. laticeps* clade [JF2018]/[JF2015]. However, in the preceding phylogeny sec. Jansen & Franz (2015), *M. imberbus* [JF2015] is non-congruently included in the *M. constrictus*-*M. imberbus* clade [JF2015]. This conflict is only resolved at the level of *Minyomerus* [JF2018]/[JF2015].

Figure 3 (**Supplemental Information SI4**) shows that the inclusion of the four new species-level concepts in the *Minyomerus* [JF2018] phylogeny generates five split-concept regions for which there are no adequate labels in either input phylogeny. These labels correspond to the overlapping articulations mentioned above; in particular the non-congruent assignments of *M. ampullaceus* [JF2018], *M. cracens* [JF2018], and *M. sculptilis* [JF2018]. The phylogenetic character evidence for these placements and relationships are discussed in the following sections.

## DISCUSSION

### Relationships to the previous revision

The differences of the current phylogeny (Figs. 37-38) in relation to that of Jansen & Franz (2015) are in large part due to the unique character combinations present in the newly added species (Rieppel 2007, Franz 2014). Nonetheless, three main clades are resolved with strong support, and further corroborate the topology of Jansen & Franz (2015), as follows:

1. *Minyomerus* [JF2018] is strongly supported by the same eight synapomorphies identified in Jansen & Franz (2015). These are reiterated in the Introduction (Bremer support value [henceforth: bsv] = 10, relative fit difference [henceforth: rfd] = 95; Bootstrap [henceforth: boot] = 100).
2. *Minyomerus griseus* [JF2015] forms a well-supported clade with *M. rutellirostris* [JF2015] (bsv = 4, rfd = 77, boot = 96). These taxa jointly share the same two synapomorphies (chars. 23:1 and 48:1) provided in Jansen & Franz (2015): (1) the intercoxal process is divided at the midpoint between the coxae, but has both the anterior and posterior processes extending completely between the procoxae and contiguous with each other; and (2) the male tergum VII is nearly 4× as long as broad, respectively. In addition, the *M. gravivultus*-*M. griseus* [JF2015] clade (bsv = 3, rfd = 60), as resolved in the current cladogram, is congruent with that of Jansen & Franz (2015).
3. *Minyomerus* [JF2018] is nested within a well-supported clade of Tanymercini [non-focal] (boot = 100). However, further work is needed to assess the phylogenetic relationships between all genera presently assigned to the Tanymercini [non-focal] (Alonso-Zarazaga & Lyal 1999).

953 **Intrageneric relationships**

954 Within *Minyomerus* [JF2018], beginning at the earliest-bifurcating node and proceeding towards the  
955 leaves, the first major incongruence with *Minyomerus* [JF2015] is the placement of *M. imberbus* [JF2015].  
956 This species was sister to the *M. constrictus*–*M. laticeps* [JF2015] clade, which in turn was sister to the  
957 *M. aeruballux*–*M. conicollis* clade [JF2015]. The present analysis places *M. imberbus* [JF2015] in a  
958 clade with *M. sculptilis* [JF2018] (see **Placement of newly described species**). The *M. aeriballux*–*M.*  
959 *imberbus* clade [JF2018] (bsf = 2, rfd = 50) is supported by three synapomorphies: (1) presence of a  
960 transverse constriction across the posterior of the frons (char. 16: 1); (2) presence of a reduced tuft of  
961 post-ocular vibrissae (char. 21: 1); and (3) a mesally obscure lamina of the spiculum ventrale in the  
962 female (char. 35: 1).

963 We resolve *M. cracens* [JF2015] as sister to the *M. aeriballux*–*M. bulbifrons* [JF2018] clade, inclusively  
964 supported by three synapomorphies: (1) presence of a strongly punctate sulcus posteriad of the nasal plate  
965 (char. 14: 2); (2) presence of broad scales on the terminal funicular segment of the antennae (char. 19: 1);  
966 and (3) absence of a medial, anteriorly-directed, sclerotized process on the coxites of the ovipositor (char.  
967 40: 1).

968 The *M. aeriballux*–*M. bulbifrons* [JF2018] clade is weakly supported by a single synapomorphy: the  
969 width of the connection between the apodemes of the aedeagal tegmen is narrower than the base of the  
970 apodeme (char. 52: 1). Within this clade, the position of the *M. bulbifrons*–*M. caseyi* clade [JF2018] clade  
971 as separate from, and sister to, the *M. aeriballux*–*M. ampullaceus* clade [JF2018], is supported by one  
972 synapomorphy and one homoplasious character, namely: (1) presence of an anterior ventral flange on the  
973 style of the spiculum gastrale (char. 44: 1 – synapomorphic), and (2) differentiation of the setae on the  
974 lateral portion of the elytra and on the venter from the setae on the elytral disc (char. 3: 1 – homoplasious).

975 **Placement of newly described species**

976 Clades within *Minyomerus* [JF2018] not addressed in the preceding section are identical in topology and  
977 composition to those of *Minyomerus* [JF2015], except for the addition of newly described species. Here  
978 we assess the phylogenetic placements of these species. We also discuss similarities in the biogeographic  
979 range of each species, in relation to the putative sister taxa, based on the results of species distribution  
980 modeling (see Figs. 4–7).

981 ***Minyomerus sculptilis* [JF2018]**

982 *Myriomerus sculptilis* [JF2018] is inferred as sister to *M. imberbus* [JF2015]. The *M. imberbus*–*M.*  
983 *sculptilis* clade [JF2018] (bsv = 3, rfd = 72) is supported by a single synapomorphy and two homoplasious  
984 characters: (1) corpus of spermatheca sinuate (char. 32: 1 – synapomorphic); (2) lamina of spiculum  
985 gastrale in male longer than broad and anteriorly extended along style (char. 45: 1 – homoplasious); and  
986 (3) aedeagal pedon medially sclerotized along dorsum (char. 51: 1 – homoplasious). In addition to these  
987 characters, *M. imberbus* [JF2015] and *M. sculptilis* [JF2018] share a general external gestalt, which makes  
988 separating these two species difficult, especially in damaged or worn specimens.

989 Whereas *M. sculptilis* [JF2018] is associated with big sagebrush (*Artemisia tridentata* [non-focal]),  
990 tumbleweed (*Salsola tragus* [non-focal]), and tall tumblemustard (*Sisymbrium altissimum* [non-focal]);  
991 its sister taxon *M. imberbus* [JF2015] is associated with bud sage (*Artemisia spinescens* [non-focal]).  
992 The divergence of these two species may have been driven in part by differences in host-plant use.  
993 However, this is less likely considering the generalist feeding habits of *Minyomerus* [JF2018] congeners.  
994 Conversely, their divergence may have resulted from a vicariance event, based on their present-day  
995 biogeographic distributions, which are separated by the eastern extension of the Columbia Plateau.  
996 *Minyomerus sculptilis* [JF2018] appears to be endemic to the Snake River Plain to the north, whereas *M.*  
997 *imberbus* [JF2015] has been found in the Great Basin Desert to the south.

998 ***Minyomerus tylotos* [JF2018]**

999 *Minyomerus tylotos* [JF2018] is sister to *M. microps* [JF2015]. The *M. microps*–*M. tylotos* clade [JF2018]  
1000 (bsv = 3, rfd = 73) is supported by a single synapomorphy and a single homoplasious character: (1) elytra  
1001 and pronotum generally large, protuberant, and sculpted in appearance along dorsal and lateral faces (char.  
1002 5: 1 – synapomorphic); and (2) sulcus posteriad of nasal plate broad and weakly punctate (char. 13: 1 –  
1003 homoplasious). In addition to these characters, the two species share a similar gestalt and uniform setation.

1004 *Minyomerus tylotos* [JF2018] appears to be endemic to northern Chihuahuan Desert, whereas *M.*  
1005 *microps* [JF2015] is widely distributed to the north throughout the Great Plains and along the Missouri

1006 River. We consider it likely that *M. microps* [JF2015] represents a northern radiation of the common  
1007 ancestor of this clade. Conversely, *M. tylotos* [JF2018] may represent the ancestral distribution to the  
1008 south, based on the hypothesized origin of *Minyomerus* [JF2018] in the Chihuahuan Desert; see Jansen &  
1009 Franz (2015) and Wilson & Pitts 2010.

1010 ***Minyomerus ampullaceus* [JF2018]**

1011 *Minyomerus ampullaceus* [JF2018] is sister to the *M. aeriballux*–*M. reburrus* clade [JF2015]. The *M.*  
1012 *aeriballux*–*M. ampullaceus* clade [JF2018] (bsv = 1, rfd = 50) is supported by a single synapomorphy:  
1013 lamina of spiculum ventrale with laminar arms basally bifurcating and sub-parallel mesally thereafter  
1014 (char. 37: 1). The placement of this species is tentative and based on the characteristics of a single, worn  
1015 specimen.

1016 Nonetheless, the biogeographic distributions of the species in the *M. aeriballux*–*M. ampullaceus*  
1017 clade [JF2018] exhibit overlap. *Minyomerus ampullaceus* [JF2018] is documented from Carlsbad, New  
1018 Mexico, in the western parts of the distributions of *M. aeriballux* [JF2015] and *M. reburrus* [JF2015].  
1019 The divergence of the latter two species is thought to be a result of their habitat and host plant preference,  
1020 given their overlapping ranges. *Minyomerus aeriballux* [JF2015] is found in very sandy soils and on  
1021 dune systems, whereas *M. reburrus* [JF2015] prefers arid grasslands. Without additional distributional or  
1022 host plant data for *M. ampullaceus* [JF2018], we cannot assess whether the single documented locality  
1023 for this species represents the center or edge of its range. However, this locality does overlap with the  
1024 known range of its sister clade, suggesting that the divergence of *M. ampullaceus* [JF2018] from the *M.*  
1025 *aeriballux*–*M. ampullaceus* clade [JF2018] was not a vicariance event.

1026 ***Minyomerus franko* [JF2018]**

1027 *Minyomerus franko* [JF2018] is sister to the *M. caseyi*–*M. trisetosus* clade [JF2015]. The *M. caseyi*–*M.*  
1028 *franko* clade [JF2018] (bsv = 4, rfd = 63) is supported by a single synapomorphy and two homoplasious  
1029 characters: (1) rows of setae on elytral intervals comprised of larger white setae randomly interspersed  
1030 among smaller brown setae(char. 4: 1 – synapomorphic); (2) prementum lacking strong ligula and  
1031 straight margins, not appearing pentagonal (char. 7: 0 – homoplasious); and (3) anterior margin of female  
1032 tergum VII entirely free of sclerotized band (char. 41: 1 – homoplasious). In addition to these characters,  
1033 members of this clade share a generally similar gestalt, especially regarding the head and rostrum, and the  
1034 articulation between the pronotum and elytra in dorsal and lateral view. The interspersed, white elytral  
1035 setae of these three species exhibit varying degrees of apical expansion, and can appear moderately to  
1036 greatly explanate or spatulate in at least some, but not all, specimens.

1037 *Minyomerus franko* [JF2018] has been documented on spear globemallow *Sphaeralcea hastulata*  
1038 [non-focal]. *Minyomerus trisetosus* [JF2015] is associated with broomweed *Xanthocephalum* [non-focal],  
1039 creosote bush *Larrea tridentata* [non-focal] and snakeweed *Gutierrezia* [non-focal]. *Minyomerus caseyi*  
1040 has no known plant associations. It is therefore possible that the divergence of *M. franko* [2018] was  
1041 facilitated by differences in host-plant preference. However, this remains unlikely given the generalist  
1042 feeding habits of congeners.

1043 Alternatively, the speciation sequence in the *M. caseyi*–*M. franko* clade [JF2018] may correspond to  
1044 vicariance events. *Minyomerus trisetosus* [JF2015] inhabits a broad swath of the northern Chihuahuan  
1045 Desert, whereas *M. franko* [JF2018] and *M. caseyi* [JF2015] are exclusively encountered in the southern  
1046 Chihuahuan Desert. MaxEnt predicts overlapping species distributions for the latter two species. However,  
1047 the *documented* localities of these two species pertain to distinct biogeographic regions. *Minyomerus*  
1048 *franko* [JF2018] has only been collected in the valleys of the Sierra Madre Oriental range, whereas  
1049 *M. caseyi* [JF2015] is found along the western edge of this range, in the eastern portion of the Central  
1050 Mexican Plateau. Additional occurrence records are needed to clarify the spatial extents of these species'  
1051 distributions, and thus draw more robust inferences regarding their endemicity.

1052 **CONCLUSIONS**

1053 Through addition of four herein described species, the entimine [non-focal] genus *Minyomerus* [JF2018]  
1054 is expanded to include 21 species. We predict that additional undescribed species of *Minyomerus* [JF2018]  
1055 exist throughout the North American deserts, given the narrow endemicity patterns of many members  
1056 of the genus. Furthermore, we believe that sampling in poorly-sampled locales, particularly in the  
1057 northwestern United States and in northern Mexico, will yield new evolutionary insights for this group.

1058 New molecular data can strengthen phylogenetic hypotheses and provide estimates regarding the timing  
1059 of diversification of *Minyomerus* [JF2018], thereby testing our current inference of an origin in central  
1060 Mexico. Another research direction should focus on the reproductive behavior of certain species suspected  
1061 to be parthenogenetic; including rearing and karyotyping. Finally, the validity of the genus *Minyomerus*  
1062 [JF2018] as a member of the Tanymecini [non-focal], and its relationships to other Entiminae [non-focal],  
1063 remain uncertain.

## 1064 ACKNOWLEDGMENTS

1065 The authors are grateful to Robert Anderson (CMNC), Ed Riley and John Oswald (TAMU), and Lourdes  
1066 Chamorro (USNM) for their assistance and provision of specimens used in this study. The authors also  
1067 thank Salvatore Anzaldo, Andrew Johnston, Sangmi Lee and other ASUHIC members for their assistance  
1068 in procuring, treating, and maintaining specimen loans upon entry into the ASUHIC.

## 1069 SUPPLEMENTAL INFORMATION

1070 **SI1** Explanation of the RCC–5 alignment approach. File format: .pdf

1071 **SI2A** Input constraints for the *Minyomerus* [JF2018]/[JF2015] rank-only classification alignment. File  
1072 format: .txt

1073 **SI2B** Input visualization for the SI2A input. File format: .pdf

1074 **SI2C** Set of 114 *Maximally Informative Relations* (MIR) for the SI2A input. File format: .csv

1075 **SI2D** Alignment visualization for the SI2A input. File format: .pdf

1076 **SI3A** Input constraints for the *Minyomerus* [JF2018]/[JF2015] phylogeny alignment – whole-concept  
1077 resolution with overlap. File format: .txt

1078 **SI3B** Input visualization for the SI3A input. File format: .pdf

1079 **SI3C** Set of 925 *Maximally Informative Relations* (MIR) for the SI3A input. File format: .csv

1080 **SI3D** Alignment visualization for the SI3A input. File format: .pdf

1081 **SI4A** Input constraints for the *Minyomerus* [JF2018]/[JF2015] phylogeny alignment – split-concept  
1082 resolution. File format: .txt

1083 **SI4B** Input visualization for the SI4A input. File format: .pdf

1084 **SI4C** Set of 925 *Maximally Informative Relations* (MIR) for the SI4A input. File format: .csv

1085 **SI4D** Alignment visualization for the SI4A input. File format: .pdf

1086 **REFERENCES**

- 1087 Agnarsson, I. & Miller, J. A. (2008), 'Is ACCTRAN better than DELTRAN?', *Cladistics* **24**(6), 1032–  
1088 1038.
- 1089 Alonso-Zarazaga, M. A. & Lyal, C. H. C. (1999), *A world catalogue of families and genera of Cur-*  
1090 *culionoidea (Insecta: Coleoptera)*, Entomopraxis, Barcelona, Spain.
- 1091 Anderson, R. S. (2002), Curculionidae, in R. H. Arnett Jr., M. C. Thomas, P. E. Skelley & J. H. Frank,  
1092 eds, 'American Beetles, Volume 2, Polyphaga: Scarabaeoidea to Curculionoidea', CRC Press, Boca  
1093 Raton, FL, chapter 131, p. 722–815.
- 1094 Arnett Jr., R. H., Samuelson, G. A. & Nishida, G. M. (1993), *The insect and spider collections of the*  
1095 *world*., 2 edn, Sandhill Crane Press, Inc., Gainesville, Florida.
- 1096 Blackwelder, R. E. & Blackwelder, R. M. (1948), *Fifth Supplement, 1939 to 1947 (Inclusive) to the Leng*  
1097 *Catalogue of Coleoptera of America, North of Mexico*, Mount Vernon, Virginia.
- 1098 Boheman, C. H. (1833), 12. T. Microsus, in C. J. Schoenherr, ed., 'Genera et species curculionidum, cum  
1099 synonymia hujus familiae', Vol. 1:2, Nicolas-Edme Roret, Paris, France, pp. 523–524.
- 1100 Bouchard, P., Bousquet, Y., Davies, A. E., Alonso-Zarazaga, M. A., Lawrence, J. F., Lyal, C. H., Newton,  
1101 A. F., Reid, C. A., Schmitt, M., Ślipiński, S. A. & Smith, A. (2011), 'Family-group names in Coleoptera  
1102 (Insecta)', *ZooKeys* **88**, 1–972.
- 1103 Bremer, K. A. (1994), 'Branch support and tree stability', *Cladistics* **10**(3), 295–304.
- 1104 Brown, R. W. (1956), *Composition of scientific words*, Smithsonian Institution Press, Washington, DC.
- 1105 Casey, T. L. (1889), 'On some new north american rhynchophora', *Annals of the New York Academy of*  
1106 *Sciences* **4**(1), 229–296.
- 1107 Chen, M., Yu, S., Franz, N., Bowers, S. & Ludäscher, B. (2014), 'Euler/x: A toolkit for logic-based  
1108 taxonomy integration', *arXiv* **1402**(1992), 1–8.
- 1109 de la Torre-Bueno, J. R., Nichols, S. W. & Tulloch, G. S. (1989), *Torre-Bueno glossary of entomology*,  
1110 New York Entomological Society in cooperation with the American Museum of Natural History, New  
1111 York City, New York.
- 1112 Elith, J., Phillips, S. J., Hastie, T., Dudík, M., Chee, Y. E. & Yates, C. J. (2011), 'A statistical explanation  
1113 of MaxEnt for ecologists', *Diversity and distributions* **17**(1), 43–57.
- 1114 Farris, J. S. (1989), 'The retention index and the rescaled consistency index', *Cladistics* **5**(4), 417–419.
- 1115 Franz, N. M. (2010a), 'Redescriptions of critical type species in the *Eustylini* Lacordaire (Coleoptera:  
1116 Curculionidae: Entiminae)', *Journal of Natural History* **44**(1–2), 41–80.
- 1117 Franz, N. M. (2010b), 'Revision and phylogeny of the Caribbean weevil genus *Apotomoderes* Dejean,  
1118 1834 (Coleoptera, Curculionidae, Entiminae).', *ZooKeys* **49**.
- 1119 Franz, N. M. (2012), 'Phylogenetic reassessment of the *Exophthalmus* genus complex (Curculionidae:  
1120 Entiminae: Eustylini, Geonemini)', *Zoological Journal of the Linnean Society* **164**(3), 510–557.
- 1121 Franz, N. M. (2014), 'Anatomy of a cladistic analysis', *Cladistics* **30**(3), 294–321.
- 1122 Franz, N. M., Chen, M., Kianmajd, P., Yu, S., Bowers, S., Weakley, A. S. & Ludäscher, B. (2016b),  
1123 'Names are not good enough: Reasoning over taxonomic change in the andropogon complex', *Semantic*  
1124 *Web (IOS)* **7**(6), 645–667.
- 1125 Franz, N. M., Musher, L. J., Brown, J. W., Yu, S., hen, M., Yu, S. & Ludäscher, B. (2018), 'Verbalizing  
1126 phylogenomic conflict: Representation of node congruence across competing reconstructions of the  
1127 neoavian explosion', *bioRxiv* pp. 1–52. <https://doi.org/10.1101/233973>.
- 1128 Franz, N. M. & Peet, R. K. (2009), 'Towards a language for mapping relationships among taxonomic  
1129 concepts', *Systematics and Biodiversity* **7**(1), 5–20.
- 1130 Franz, N. M., Pier, N. M., Reeder, D. M., Chen, M., Yu, S., Kianmajd, P., Bowers, S. & Ludäscher, B.  
1131 (2016a), 'Two influential primate classifications logically aligned', *Systematic Biology* **65**(4), 561–582.
- 1132 Goloboff, P. A. (1999), *NONA - Version 2.0 (for Windows)*. <http://www.cladistics.com>.
- 1133 Goloboff, P. A. & Farris, J. S. (2001), 'Methods for quick consensus estimation', *Cladistics* **17**(1), S26–  
1134 S34.
- 1135 Goloboff, P. A., Farris, J. S. & Nixon, K. C. (2008), 'Tnt, a free program for phylogenetic analysis',  
1136 *Cladistics* **24**(5), 774–786.
- 1137 Google Inc. (2018), *Google Earth Pro - Version 7.3.1.4507*. <https://www.google.com/earth/>.
- 1138 Green, J. W. (1920), 'Notes on American Rhynchophora (Col.)', *Entomological News* **31**, 193–201.
- 1139 Hijmans, R. J., Cameron, S. E., Parra, J. L., Jones, P. G. & Jarvis, A. (2005), 'Very high resolution  
1140 interpolated climate surfaces for global land areas', *International journal of climatology* **25**(15), 1965–

1978.

Hijmans, R. J., Garcia, N., Kapoor, J., Rala, A., Maunahan, A. & Wieczorek, J. (2012), *Global administrative areas (boundaries)*, Museum of Vertebrate Zoology and the International Rice Research Institute, University of California, Berkeley, California. <http://www.gadm.org/>.

Horn, G. H. (1876), Family V. OTIORHYNCHIDÆ, in J. L. LeConte & G. H. Horn, eds, 'The Rhynchophora of America, north of Mexico', Vol. 15, Proceedings of the American Philosophical Society, New York City, New York, pp. 13–112.

Howden, A. T. (1959), 'A revision of the species of *Pandeleteius* Schönherr and *Pandeleteinus* Champion of America north of Mexico: (Coleoptera: Curculionidae)', *Proceedings of the California Academy of Sciences* **29**, 361–421.

Howden, A. T. (1970), 'The Tanymecini of the West Indies (Coleoptera: Curculionidae)', *Contributions of the American Entomological Institute* **5**, 1–73.

Howden, A. T. (1982), 'Revision of the New World genus *Hadromeropsis* Pierce (Coleoptera, Curculionidae, Tanymecini)', *Contributions of the American Entomological Institute* **19**, 1–180.

Howden, A. T. (1995), 'Structures related to oviposition in Curculionoidea', *Memoirs of the Entomological Society of Washington* **14**, 53–100.

Jansen, M. A. & Franz, N. M. (2015), 'Phylogenetic revision of *Minyomerus* Horn, 1876 sec. Jansen and Franz, 2015 (Coleoptera: Curculionidae) using taxonomic concept annotations and alignments', *ZooKeys* **528**, 1–133.

Kissinger, D. G. (1964), *Curculionidae of America North of Mexico. A Key to the Genera*, Taxonomic Publications, South Lancaster, Massachusetts.

LeConte, J. L. (1859), *The Complete Writings of Thomas Say on the Entomology of North America*, Baillière Brothers, London, England.

LeConte, J. L. & Horn, G. H. (1876), 'The Rhynchophora of America, north of Mexico', *Proceedings of the American Philosophical Society* **15**(96), 1–455.

Marvaldi, A. E. (1997), 'Higher level phylogeny of Curculionidae (Coleoptera: Curculionoidea) based mainly on larval characters, with special reference to broad-nosed weevils', *Cladistics* **13**(4), 285–312.

Marvaldi, A. E., Lanteri, A. A., del Río, M. G. & Oberprieler, R. G. (2014), Entiminae Schoenherr, 1823, in R. A. B. Leschen & R. G. Beutel, eds, 'Handbook of Zoology: Arthropoda: Insecta: Coleoptera Volume 3: Morphology and Systematics (Phytophaga)', De Gruyter, Berlin, Germany, chapter 3.7.5, p. 503–522.

Morimoto, K. & Kojima, H. (2003), 'Morphologic characters of the weevil head and phylogenetic implications (Coleoptera, Curculionoidea)', *Esakia* **43**, 133–169.

Munz, P. A. & Keck, D. D. (1973), *A Californian flora (with supplement)*, University of California Press, Berkeley, California.

Nixon, K. C. (2002), *WinClada - Version 1.00. 08*. <http://www.diversityoflife.org/winclada/>.

Nixon, K. C. & Carpenter, J. M. (1993), 'On outgroups', *Cladistics* **9**(4), 413–426.

Oberprieler, R. G., Anderson, R. S. & Marvaldi, A. E. (2014), Curculionoidea Latreille, 1802: Introduction, Phylogeny, in R. A. B. Leschen & R. G. Beutel, eds, 'Handbook of Zoology: Arthropoda: Insecta: Coleoptera Volume 3: Morphology and Systematics (Phytophaga)', De Gruyter, Berlin, Germany, chapter 3, pp. 285–300.

Oberprieler, R. G., Marvaldi, A. E. & Anderson, R. S. (2007), 'Weevils, weevils, weevils everywhere', *Zootaxa* **1668**(1), 491–520.

O'Brien, C. W. & Wibmer, G. J. (1982), *Annotated checklist of the weevils (Curculionidae sensu lato) of North America, Central America, and the West Indies (Coleoptera: Curculionoidea)*, American Entomological Institute, Ann Arbor, Michigan.

Phillips, S. J., Anderson, R. P. & Schapire, R. E. (2006), 'Maximum entropy modeling of species geographic distributions', *Ecological modelling* **190**(3–4), 231–259.

Phillips, S. J., Dudík, M. & Schapire, R. E. (2004), A maximum entropy approach to species distribution modeling, in 'Proceedings of the 21st International Conference on Machine Learning', ACM, pp. 83–90.

Pierce, W. D. (1909), 'Studies of North American weevils', *Proceedings of the United States National Museum* **37**(1708), 325–364.

Pierce, W. D. (1913), 'Miscellaneous contributions to the knowledge of the weevils of the families Attelabidae and Brachyrhinidae', *Proceedings of the United States National Museum* **45**(1988), 365–426.

- 1196 Quantum GIS Development Team (2018), ‘Quantum GIS Geographic Information System’, *Open Source*  
1197 *Geospatial Foundation Project*. <http://qgis.osgeo.org>.
- 1198 Rieppel, O. (2007), ‘The performance of morphological characters in broad-scale phylogenetic analyses’,  
1199 *Biological Journal of the Linnean Society* **92**(2), 297–308.
- 1200 Say, T. (1831), Descriptions of North American Curculionides and an arrangement of some of our known  
1201 species agreeably to the method of Schoenherr, in J. L. LeConte, ed., ‘The Complete Writings of  
1202 Thomas Say on the Entomology of North America’, Vol. 1, Baillière Brothers, London, England,  
1203 pp. 1–30.
- 1204 SEINet (2018), *Southwest Environmental Information Network*. <http://swbiodiversity.org/seinet/index.php>.
- 1205 Sharp, D. (1891), Coleoptera. Rhynchophora. Curculionidae. Attelabinae, Pterocolinae, Allocoryninae,  
1206 Apioninae, Thecesterninae, Otiorhynchinae [part, “Apterae”], in D. Sharp & G. C. Champion, eds,  
1207 ‘Biologia Centrali-Americanica’, Vol. 4:3, London, England, pp. 87–177.
- 1208 Sleeper, E. L. (1960), ‘Notes on the Curculionoidea II: 20. a contribution to the knowledge of the  
1209 Curculionoidea’, *Ohio Journal of Science* **60**(2), 83–88.
- 1210 Thompson, R. T. (1992), ‘Observations on the morphology and classification of weevils (Coleoptera,  
1211 Curculionoidea) with a key to major groups’, *Journal of Natural History* **26**(4), 835–891.
- 1212 Ting, P. C. (1936), ‘The mouth parts of the coleopterous group Rhynchophora’, *Microentomology*  
1213 **1**, 93–114.
- 1214 Wheeler, Q. D. & Platnick, N. I. (2000), The phylogenetic species concept (*sensu* Wheeler and Platnick),  
1215 in Q. D. Wheeler & R. Meier, eds, ‘Species Concepts and Phylogenetic Theory: a Debate’, Columbia  
1216 University Press, New York City, New York, pp. 55–69.
- 1217 Wilson, J. S. & Pitts, J. P. (2010), ‘Illuminating the lack of consensus among descriptions of earth  
1218 history data in the north american deserts: a resource for biologists’, *Progress in Physical Geography*  
1219 **34**(4), 419–441.

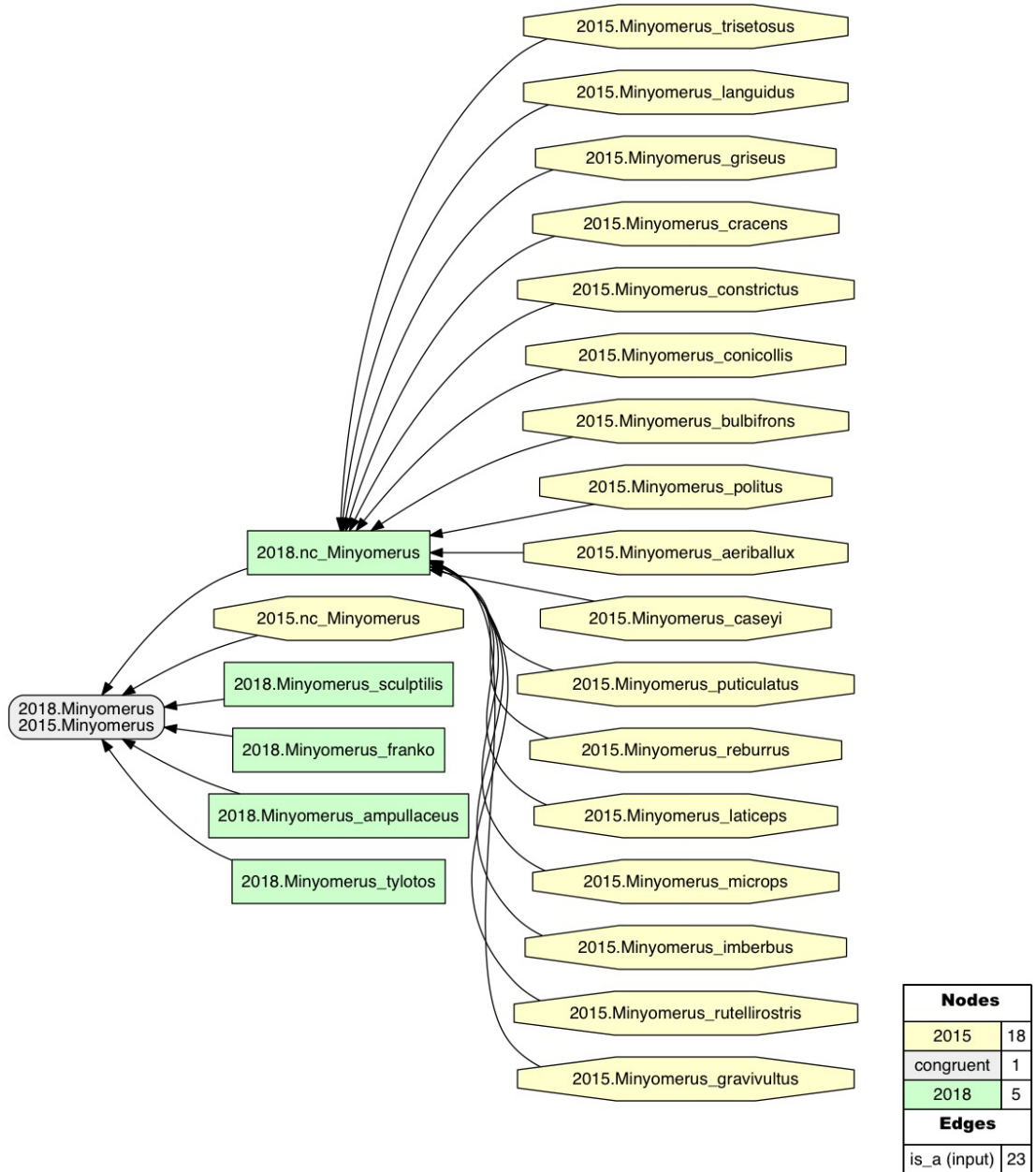


**Figure 1. Intensional RCC-5 alignment of the rank-only classifications of *Minyomerus* [JF2018]/[JF2015].** See also Jansen & Franz (2015) and Supplemental Information SI2. Taxonomic concept labels such as *Minyomerus microps* [JF2015] are abbreviated as "2015.Minyomerus\_microps". Relaxation of the coverage constraint is indicated with the prefix "nc\_" (no coverage). Congruent concept regions ( $T_2$  and  $T_1$ ) are shown as grey rectangles, concepts unique to the later taxonomy ( $T_2$ ) are shown as green rectangles, and concept regions unique to the earlier taxonomy ( $T_1$ ) are shown as yellow octagons. Articulations of inverse proper inclusion ( $<$ ) and overlap ( $><$ ), where present, are also shown.

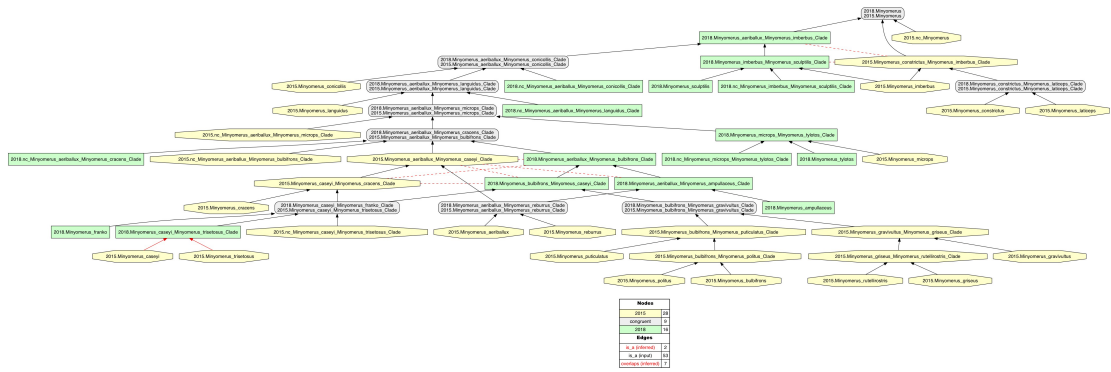


**Figure 2. Intensional RCC–5 alignment of the phylogenies of *Minyomerus* [JF2018]/[JF2015] – whole-concept resolution with overlap.** See also **Supplemental Information SI3**. Seven overlapping articulations are inferred. For further discussion, see the **RCC–5 Alignments** section.

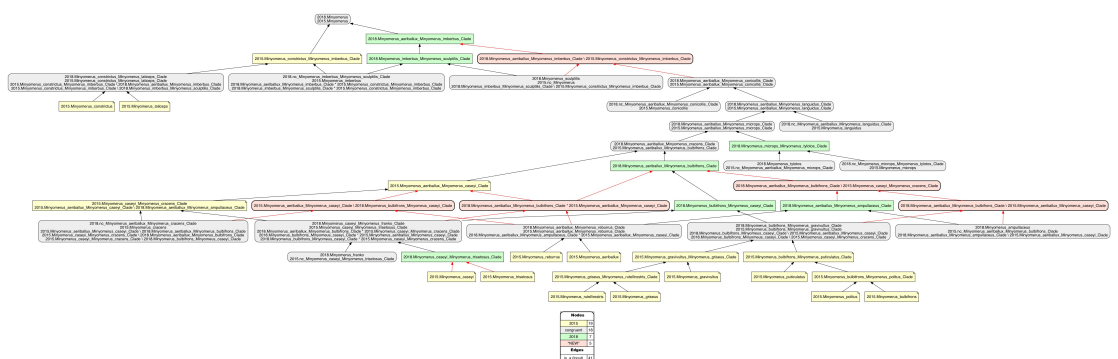


**Figure 3. Intensional RCC–5 alignment of the phylogenies of *Minyomerus* [JF2018]/[JF2015] – split-concept resolution.** See also **Supplemental Information SI4**. The seven overlapping articulations of the alignment displayed Fig. 2 are resolved into their constituent split regions. That is, if regions A and B overlap, the three resulting split regions are labeled A\B ("A, not B"), A\*B ("A and B"), and B\A ("B, not A"). Five split-concept regions can *only* be named using this convention, and are salmon-colored in the alignment visualization.

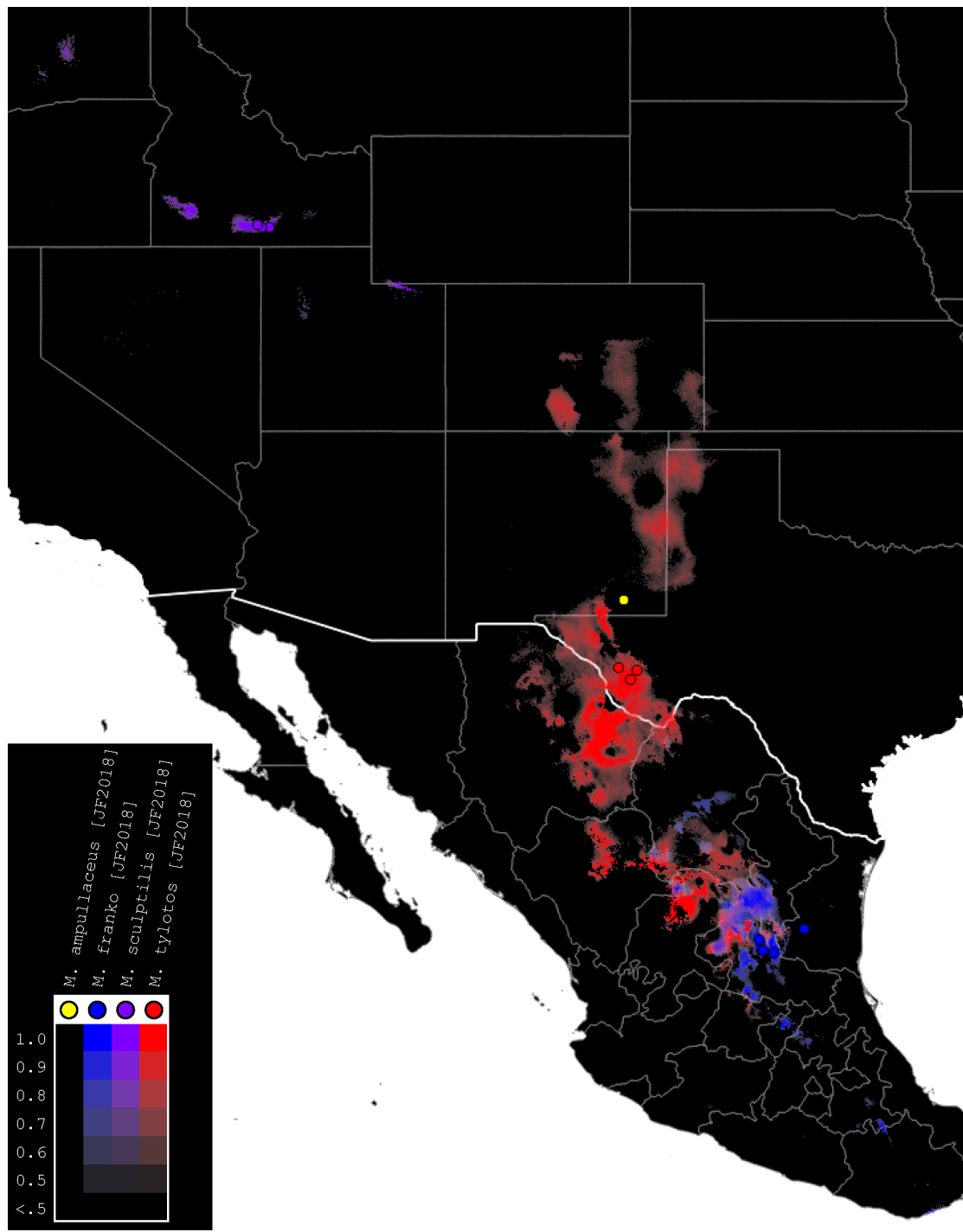


**Figure 4. Summary map of distributions of new species of *Minyomerus* [JF2018].** Combined occurrence record and Maxent habitat modeling map for four newly-described species of *Minyomerus* [JF2018], as indicated in the legend.

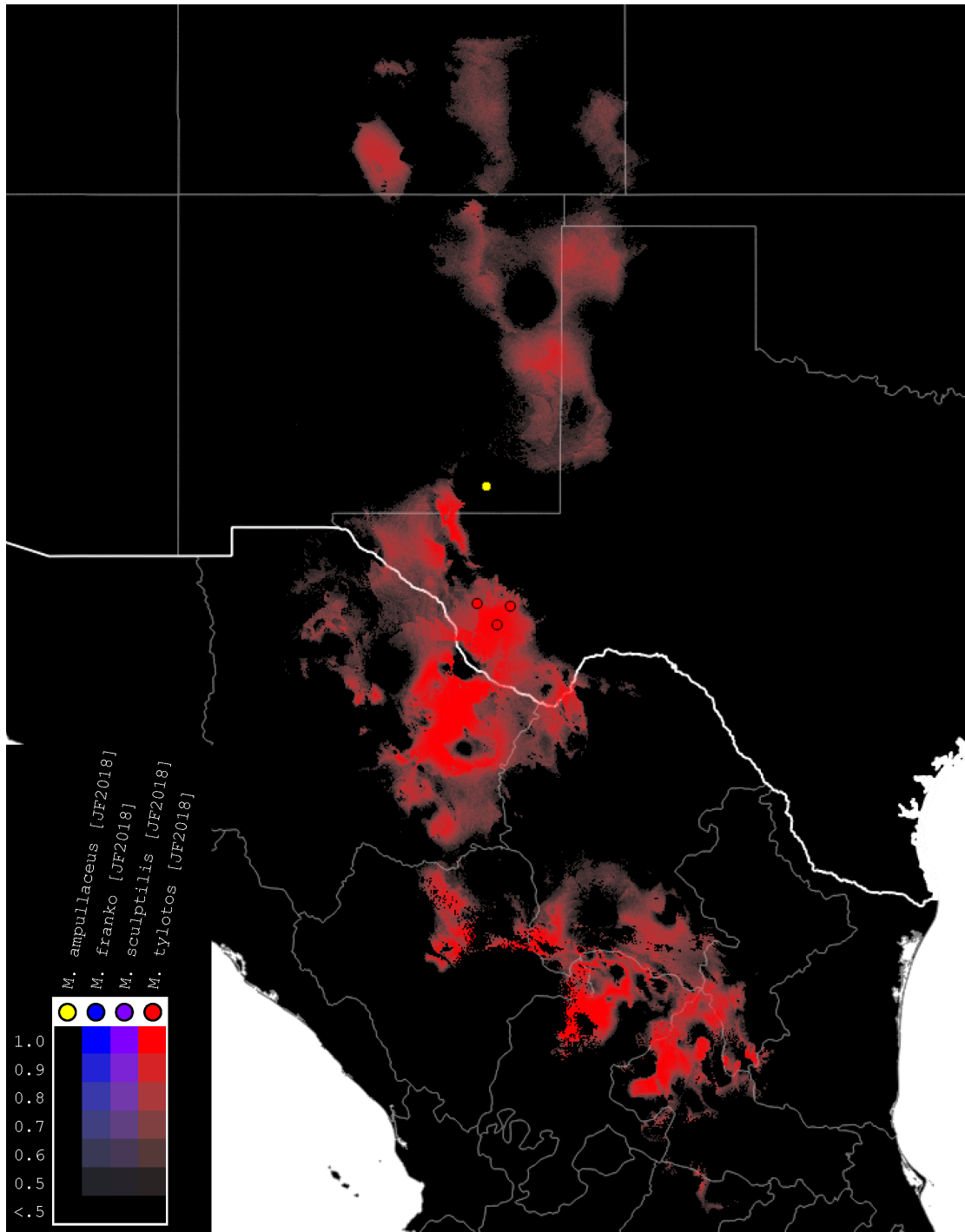


**Figure 5. Distributions of *M. ampullaceus* [JF2018] and *M. tylotos* [JF2018].** Combined occurrence record and Maxent habitat modeling map for *M. ampullaceus* [JF2018] and *M. tylotos* [JF2018], as indicated in the legend.

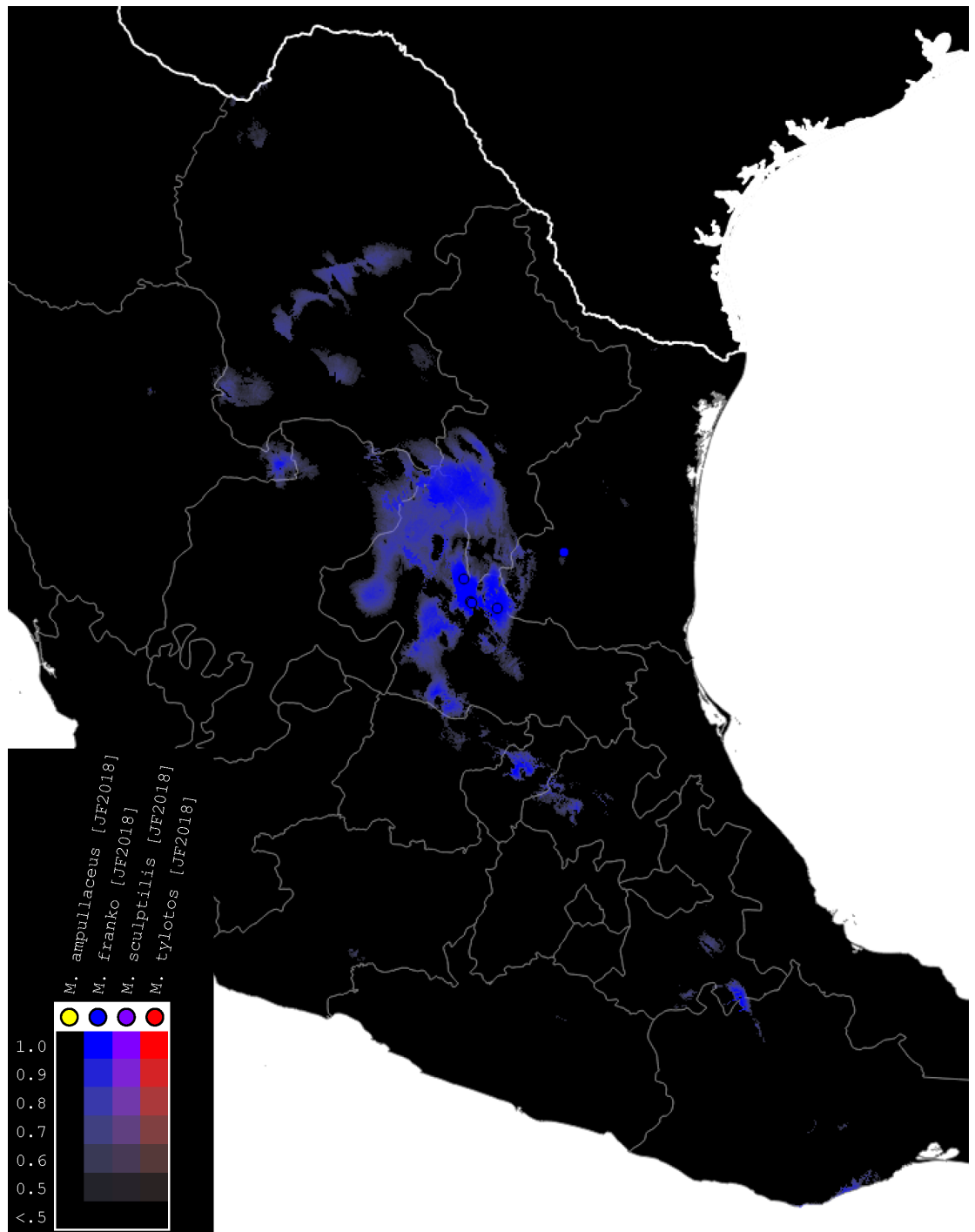


**Figure 6. Distributions of *M. franko* [JF2018].** Combined occurrence record and Maxent habitat modeling map for *M. franko* [JF2018], as indicated in the legend.

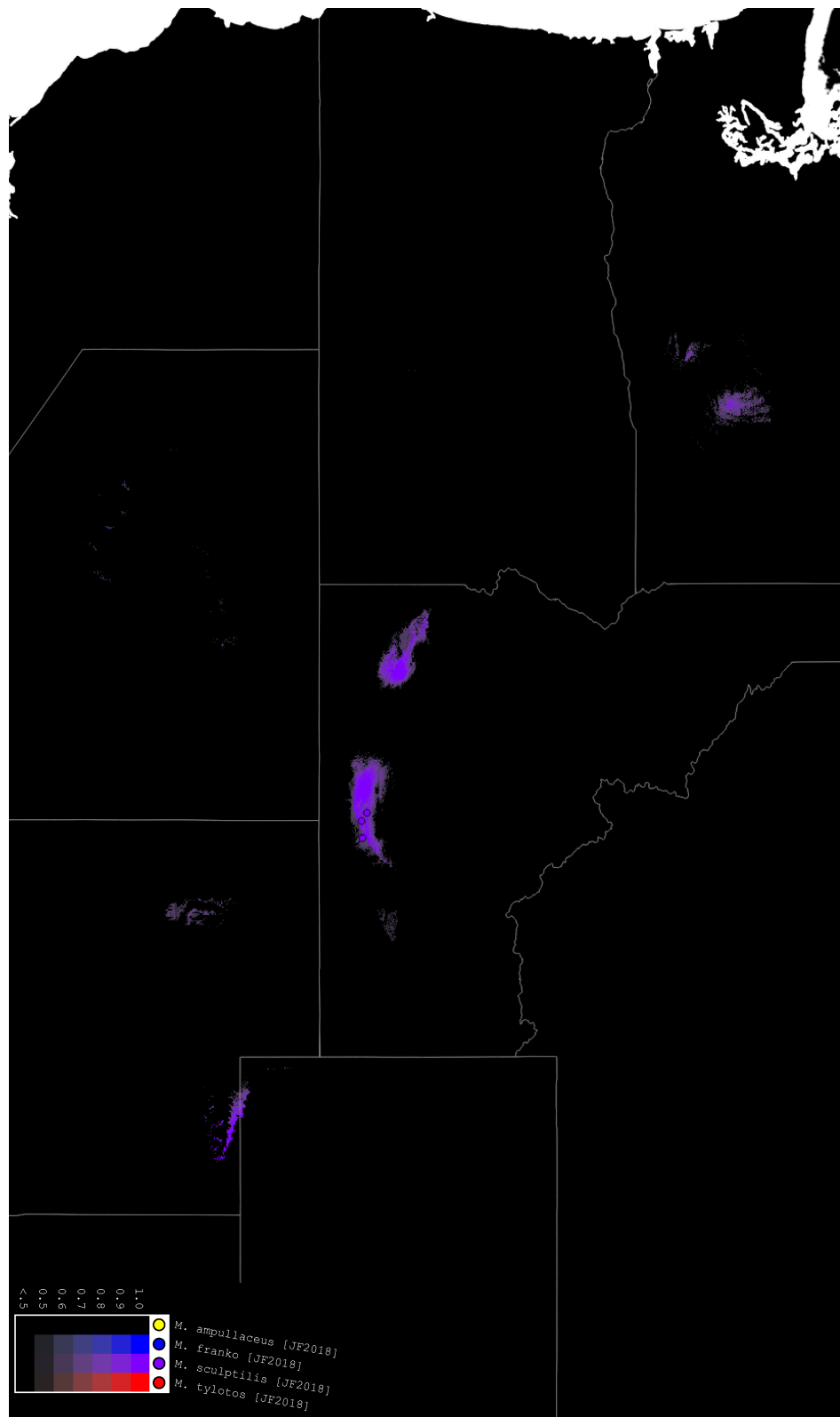


**Figure 7. Distributions of *M. sculptilis* [JF2018].** Combined occurrence record and Maxent habitat modeling map for *M. sculptilis* [JF2018], as indicated in the legend.



**Figure 8. Dorsal habitus of *M. ampullaceus* [JF2018].** Image of female (♀) holotype. Photo credit: Andrew Jansen.



**Figure 9. Lateral habitus of *M. ampullaceus* [JF2018].** Image of female (♀) holotype. Photo credit: Andrew Jansen.



**Figure 10.** Ventral habitus of *M. ampullaceus* [JF2018]. Image of female (♀) holotype. Photo credit: Andrew Jansen.



**Figure 11.** Head and rostrum of *M. ampullaceus* [JF2018]. Frontal view of female (♀) holotype.  
Photo credit: Andrew Jansen.

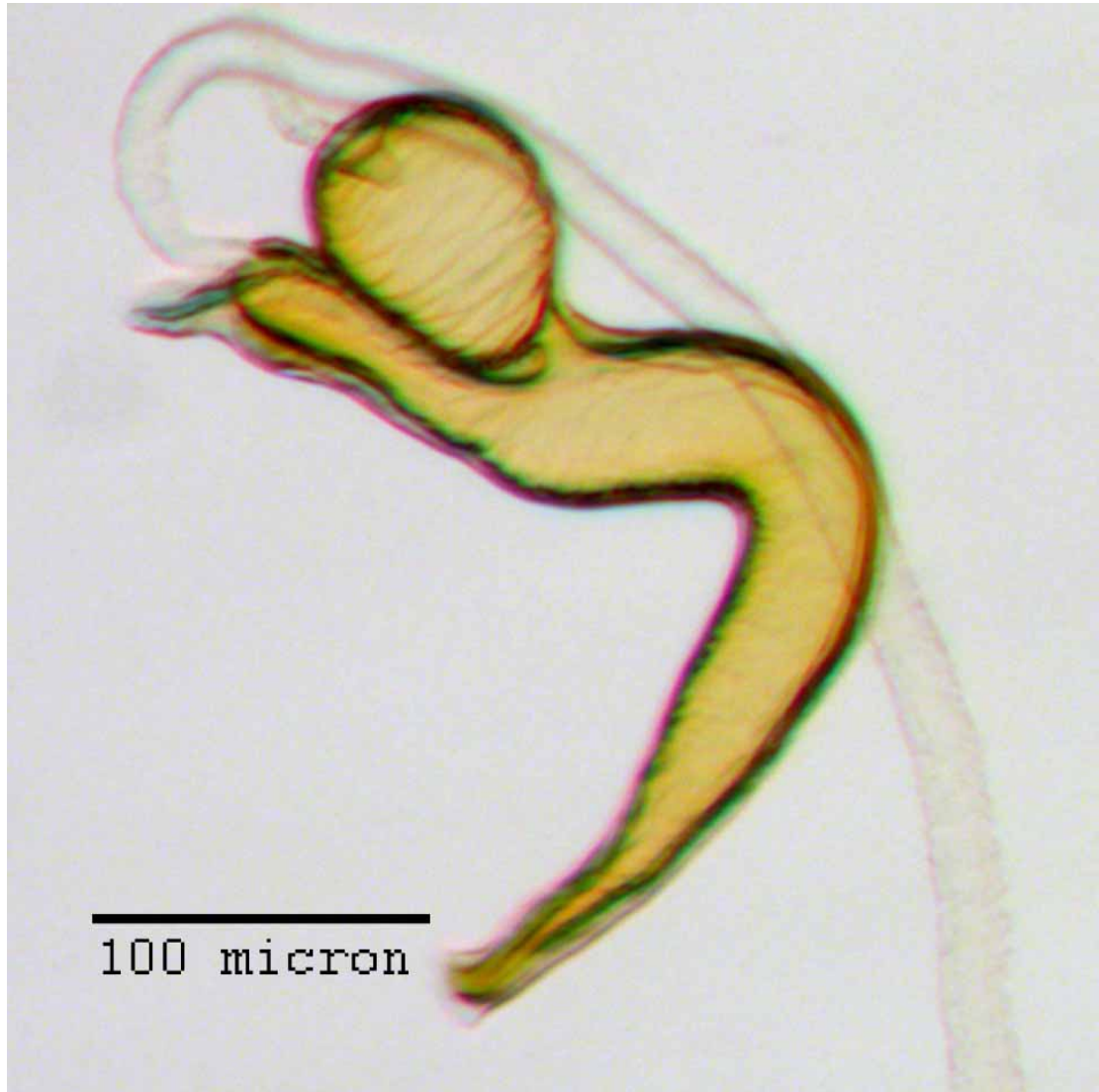


**Figure 12.** Spermatheca of *M. ampullaceus* [JF2018]. Genitalia of female (♀) holotype. Photo credit: Andrew Jansen.



**Figure 13.** Lamina of spiculum ventrale of *M. ampullaceus* [JF2018]. Sternum VIII of female (♀) holotype. Photo credit: Andrew Jansen.



**Figure 14. Dorsal habitus of *M. franko* [JF2018].** Image of female (♀) holotype. Photo credit: Andrew Jansen.



**Figure 15.** Lateral habitus of *M. franko* [JF2018]. Image of female (♀) holotype. Photo credit: Andrew Jansen.



**Figure 16.** Ventral habitus of *M. franko* [JF2018]. Image of female (♀) holotype. Photo credit: Andrew Jansen.



**Figure 17.** Head and rostrum of *M. franko* [JF2018]. Frontal view of female (♀) holotype. Photo credit: Andrew Jansen.



**Figure 18.** Maxilla of *M. franko* [JF2018]. Dextral maxilla of female (♀) paratype. Photo credit: Andrew Jansen.



**Figure 19. Prementum of *M. franko* [JF2018].** Labium of female (♀) paratype. Photo credit: Andrew Jansen.



**Figure 20.** Spermatheca of *M. franko* [JF2018]. Genitalia of female (♀) paratype. Photo credit: Andrew Jansen.

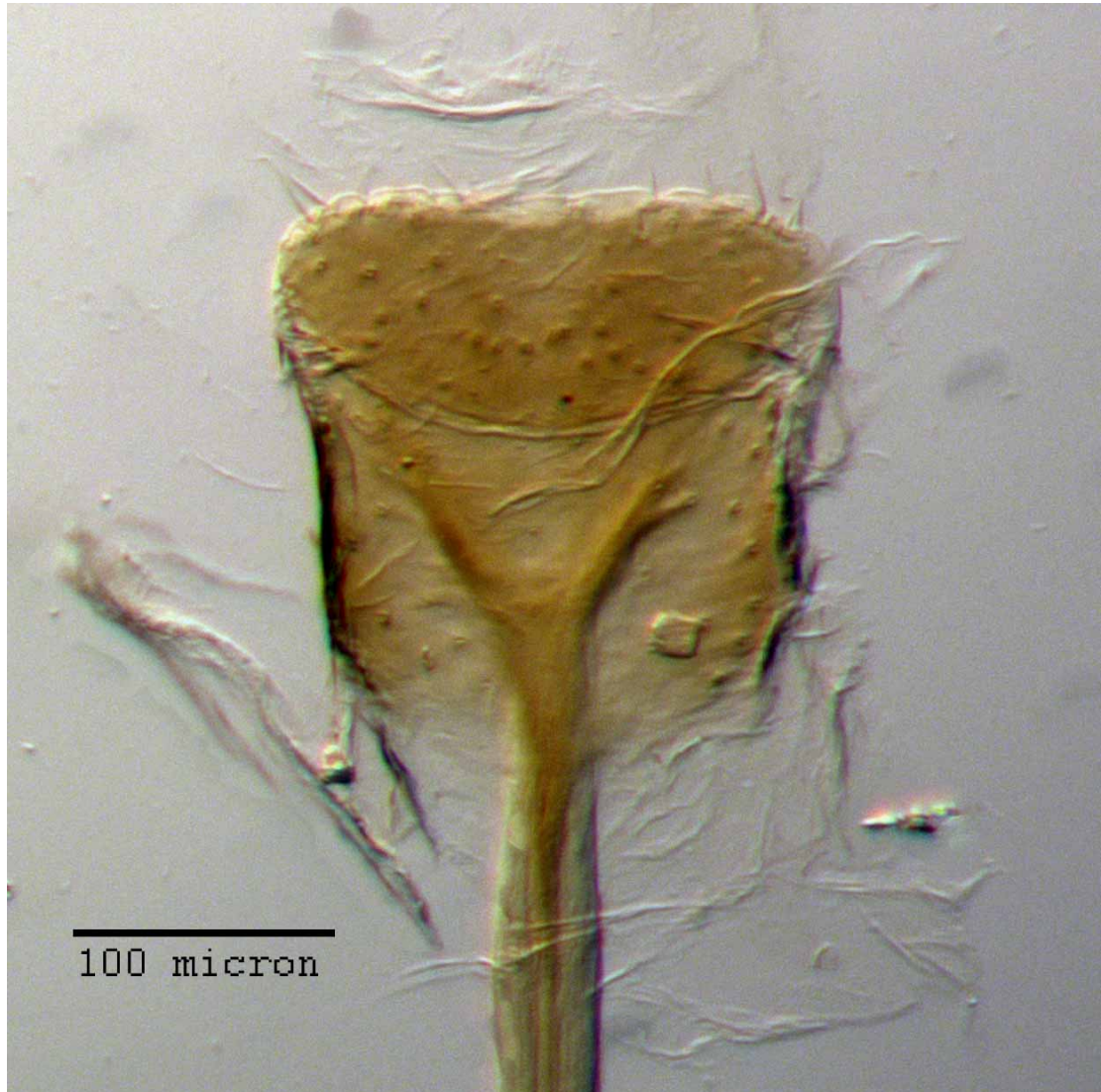


**Figure 21.** Lamina of spiculum ventrale of *M. franko* [JF2018]. Sternum VIII of female (♀) paratype. Photo credit: Andrew Jansen.



**Figure 22. Aedeagus of *M. franko* [JF2018].** Genitalia of male ( $\sigma$ ) paratype in (A) dorsal view and (B) lateral view. Photo credit: Andrew Jansen.



**Figure 23.** Dorsal habitus of *M. sculptilis* [JF2018]. Image of female (♀) holotype. Photo credit: Andrew Jansen.



**Figure 24. Lateral habitus of *M. sculptilis* [JF2018].** Image of female (♀) holotype. Photo credit: Andrew Jansen.



**Figure 25. Ventral habitus of *M. sculptilis* [JF2018].** Image of female (♀) holotype. Photo credit: Andrew Jansen.



**Figure 26. Head and rostrum of *M. sculptilis* [JF2018].** Frontal view of female (♀) holotype. Photo credit: Andrew Jansen.

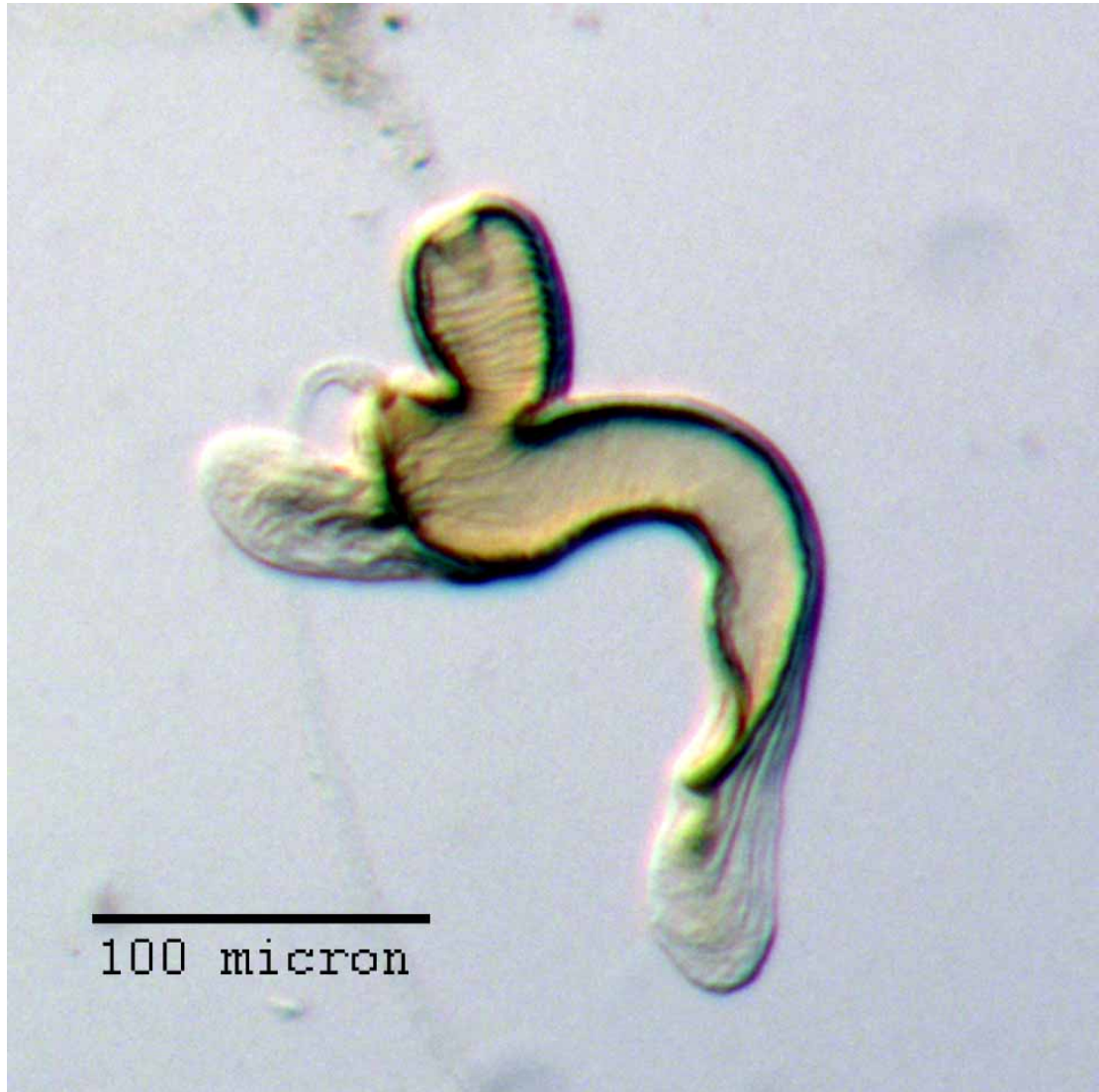


**Figure 27. Spermatheca of *M. sculptilis* [JF2018].** Genitalia of female (♀) paratype. Photo credit: Andrew Jansen.

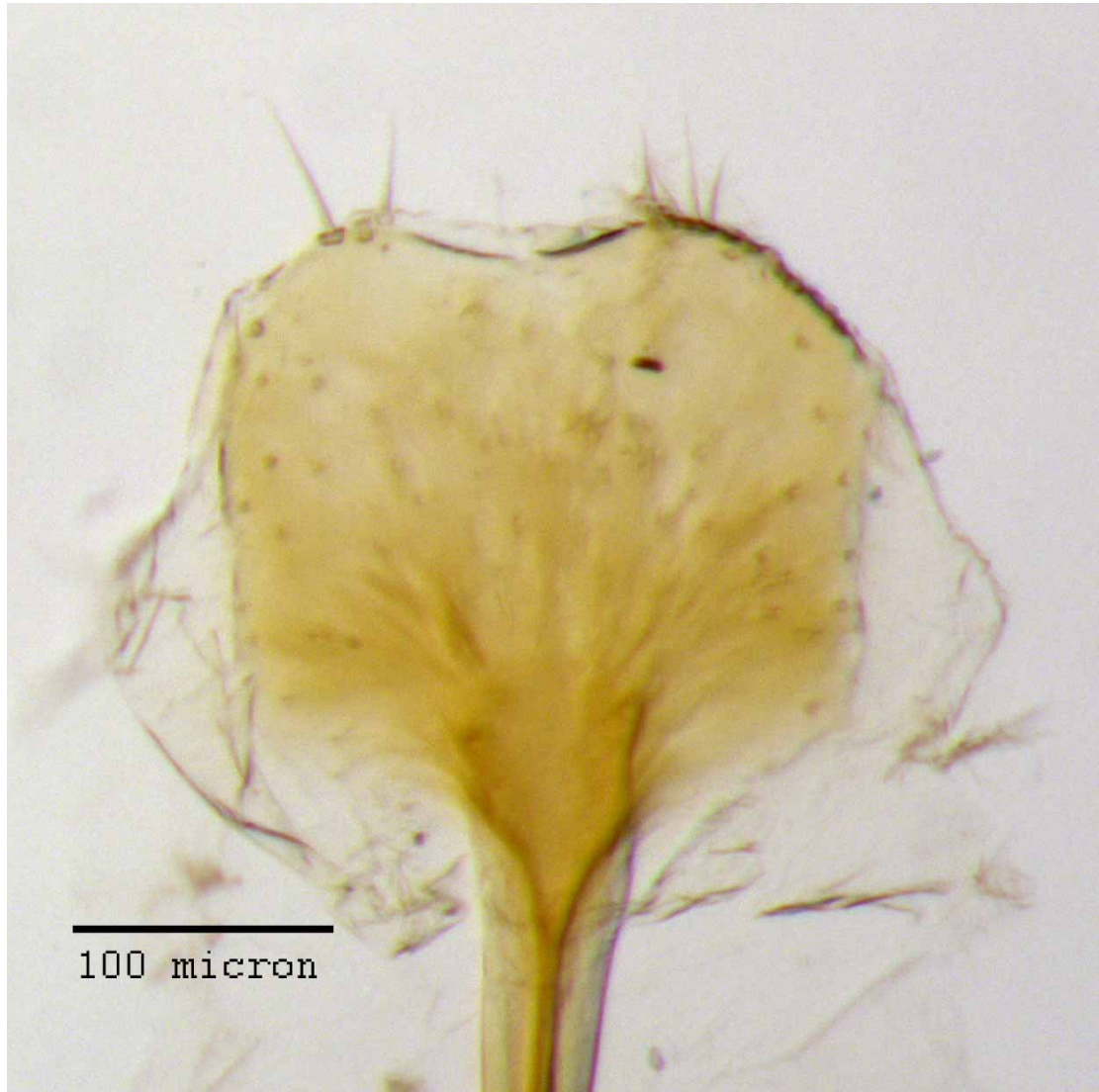


**Figure 28.** Lamina of spiculum ventrale of *M. sculptilis* [JF2018]. Sternum VIII of female (♀) paratype. Photo credit: Andrew Jansen.



**Figure 29. Aedeagus of *M. sculptilis* [JF2018].** Genitalia of male ( $\sigma$ ) paratype in (A) dorsal view and (B) lateral view. Photo credit: Andrew Jansen.



**Figure 30.** Dorsal habitus of *M. tylotos* [JF2018]. Image of female (♀) holotype. Photo credit: Andrew Jansen.



**Figure 31. Lateral habitus of *M. tylotos* [JF2018].** Image of female (♀) holotype. Photo credit: Andrew Jansen.



**Figure 32. Ventral habitus of *M. tylotos* [JF2018].** Image of female (♀) holotype. Photo credit: Andrew Jansen.



**Figure 33.** Head and rostrum of *M. tylotos* [JF2018]. Frontal view of female (♀) holotype. Photo credit: Andrew Jansen.

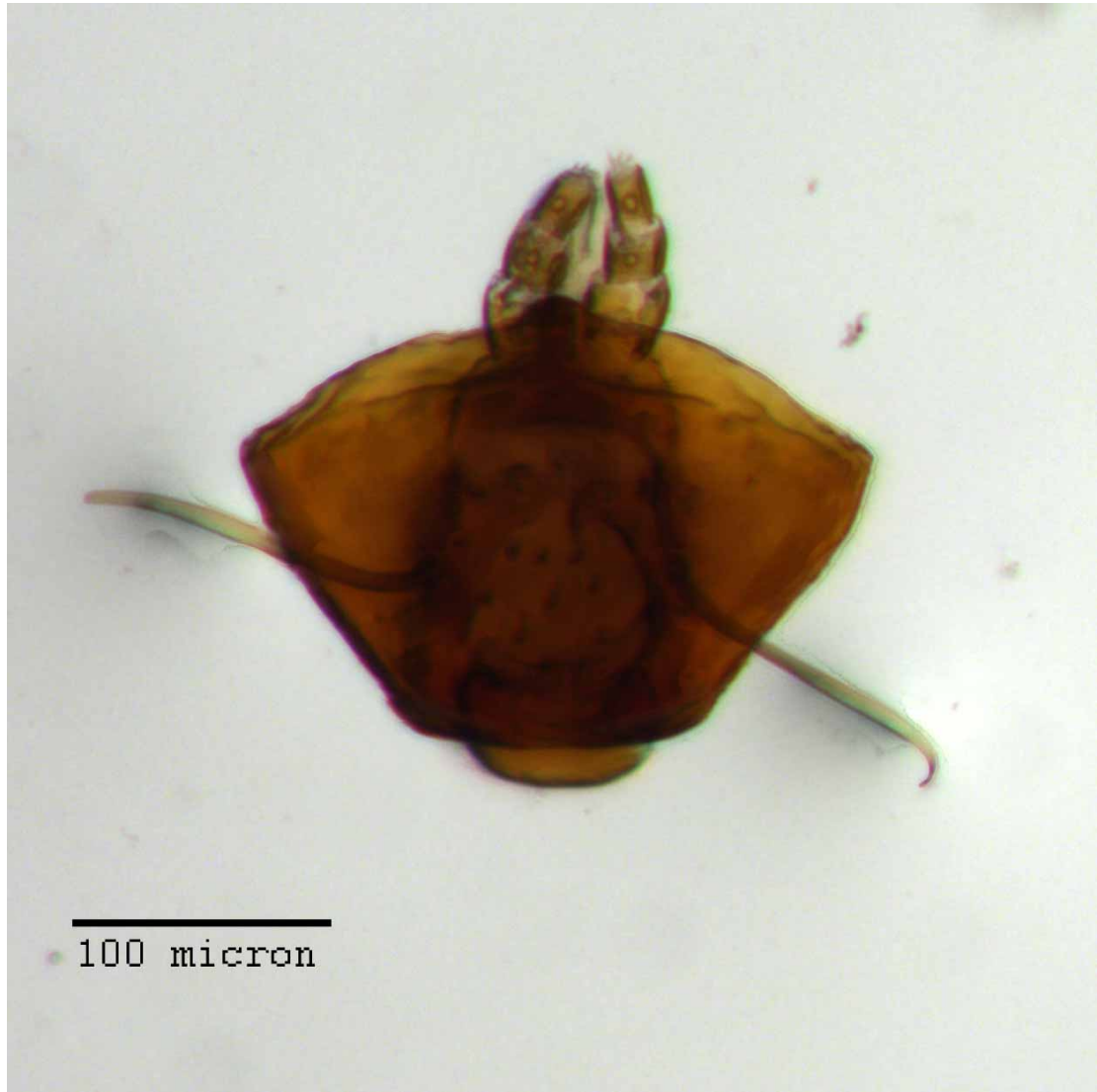


**Figure 34.** Prementum of *M. tylotos* [JF2018]. Labium of female (♀) paratype. Photo credit: Andrew Jansen.



**Figure 35.** Spermatheca of *M. tylotos* [JF2018]. Genitalia of female (♀) paratype. Photo credit: Andrew Jansen.



**Figure 36. Lamina of spiculum ventrale of *M. tylotos* [JF2018].** Sternum VIII of female (♀) paratype. Photo credit: Andrew Jansen.

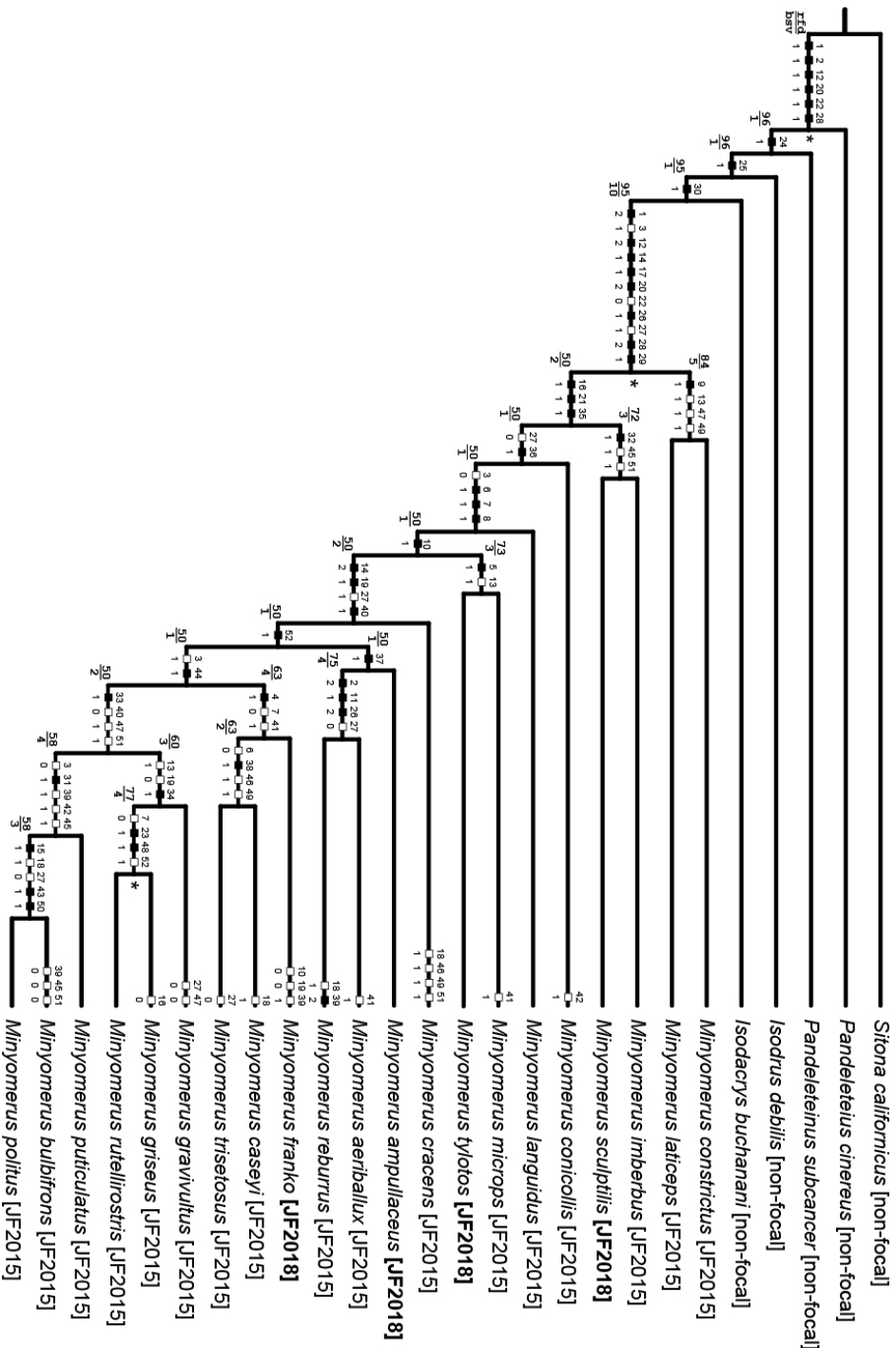


**Figure 37. Preferred phylogeny – character transitions and support.** Single most parsimonious cladogram representing the preferred phylogeny of species of *Minyomerus* [JF2018], and select outgroup taxa ( $L = 99$ ,  $CI = 60$ ,  $RI = 80$ ). Characters 9, 27, 39, 45 - 47, 49, and 51 are mapped under ACCTRAN optimization; all others are unambiguously optimized. Black squares indicate non-homoplasious character state changes, whereas white squares indicate homoplasious character state changes. The numbers above and below the squares represent character numbers and states, respectively. Bremer support (upper value) and relative fit difference (lower value) values can be found at the left ends of the branches. A "\*" symbol at the right end of a branch indicates Bootstrap support greater than 0.95.

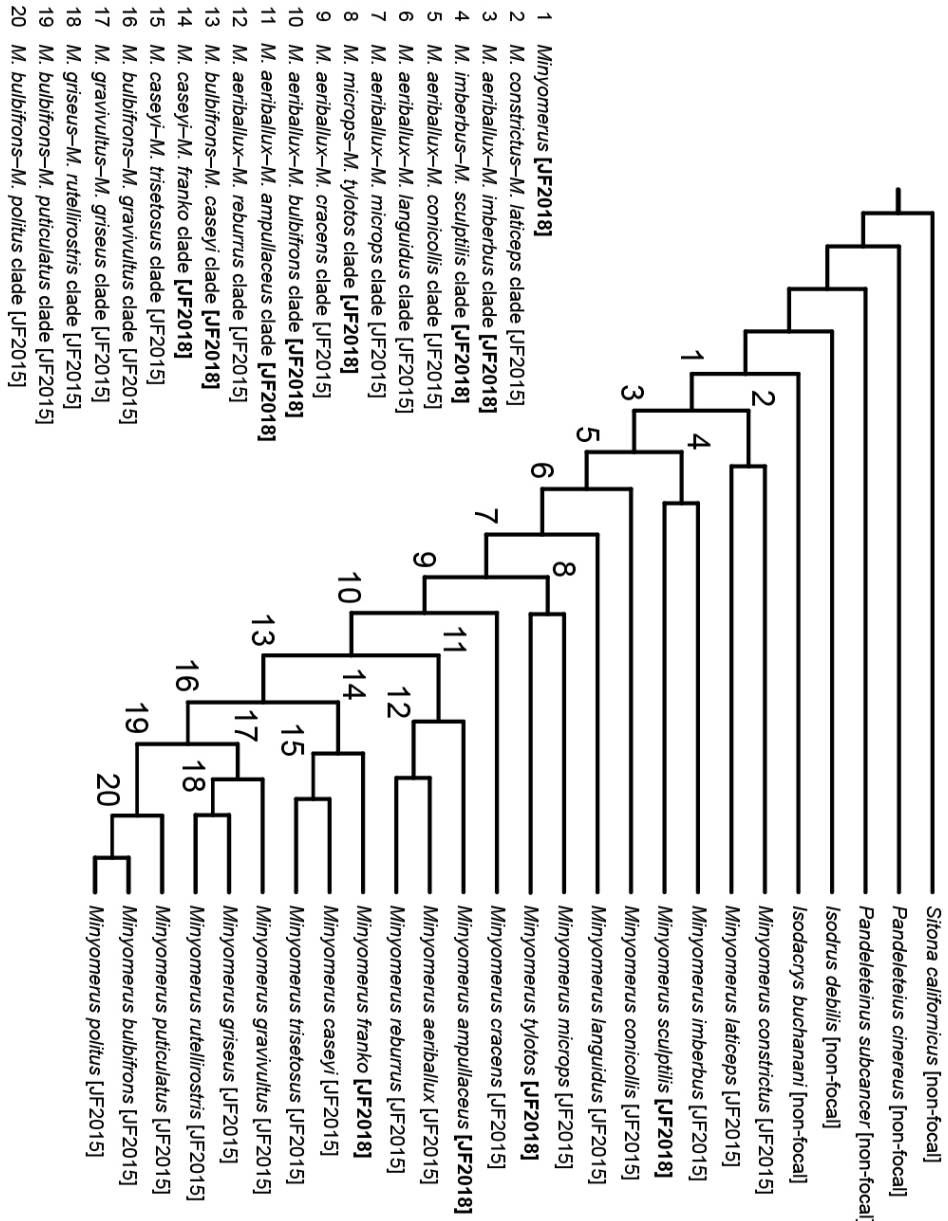


**Figure 38. Preferred phylogeny – clade concept labels.** Topology and species-level taxonomic concept labels as in Fig. 37. Clade concept labels, numbered 1-20, are consistently generated by using the alphabetically first epithet in each of the bifurcating sister clades. This method safeguards the clade concept labels against changes due simply to reorientation of leaves. Bold-font square brackets indicate new [JF2018] labels. See also **RCC-5 Alignments**.